Impact of *Streptococcus pneumoniae* biosynthesis gene mutations on epithelial microinvasion and cellular responses

Caroline M. Weight[1*], Gabriele Pollara[1], Modupeh Betts[1], Roberta Ragazzini[2], Michael Connor[3], Elisa Ramos-Sevillano[4], Jesús Reiné[5], Matthew Whelan[1], José Afonso Guerra-Assunção[1], Paola Bonfanti[1,2], Clare Jolly[1], Mahdad Noursadeghi[1], Daniela M. Ferreira[5], Jeremy S. Brown[4], Robert S. Heyderman[1]

[1]Research Department of Infection, Division of Infection and Immunity, UCL London, UK

[2]Francis Crick Institute, London, UK

[3]Chromatin and Infection, Institut Pasteur, France

[4]Department of Respiratory Medicine, UCL, London, UK

[5]Oxford Vaccine Group, University of Oxford, Oxford and Clinical Sciences, Liverpool School of Tropical Medicine, Liverpool, UK

*Current address Biomedical and Life Sciences, Faculty of Health and Medicine, Lancaster University, UK

Corresponding Authors: Dr Caroline M. Weight

Email: c.weight@ucl.ac.uk

ABSTRACT

Epithelial cells are important gatekeepers during bacterial colonisation of the nasopharynx by *Streptococcus pneumoniae.* The bacterial and host factors influencing the outcomes of this interaction are poorly understood but there is increasing recognition that bacterial metabolism is an important determinant of virulence. Pneumococcal colonisation is associated with microcolony formation and epithelial microinvasion without disease in healthy individuals. We have assessed the impact of mutations in two *S. pneumoniae* biosynthesis genes, glutamate 5 kinase (*proABC*) and formate tetrahydrofolate reductase (*fhs*) on epithelial cell microinvasion and subsequent epithelial-innate immunity, using an Experimental Human Pneumococcal Challenge (EHPC) model, primary NHBE-A healthy human bronchial epithelial cells and Detroit 562 nasopharyngeal cells.

Bacterial transcriptomic analysis revealed profound effects to stress response following deletion of *proABC* or *fhs* genes. Mutant strains retained the ability to colonise in the EHPC model. By day 6 post-inoculation, a higher proportion of mutant strains were found inside epithelial cells compared to WT. In primary epithelial cells, microscopy analyses revealed epithelial surface differences between strains, with enhancement of acetylated tubulin (a marker of Ciliated cells) and β catenin expression following Δ*proABC/piaA* exposure and enhancement of uteroglobin (a marker of Clara cells) expression following Δ*fhs/piaA* exposure. In Detroit 562 cells, pneumococcal adhesion was reduced ten-fold for both the Δ*proABC/piaA* and Δ*fhs/piaA* strains compared to WT. Microinvasion was four times higher for the mutants compared to WT. In Detroit 562 cells, the WT and Δ*proABC/piaA* strains induced a similar epithelial transcriptomic response, dominated by inflammatory response genes, distinct from the response to Δ*fhs/piaA* strain, which primarily induced upregulation of cellular stress and repair genes. Insights into differential activation of caspase pathways following infection with the different strains shed light on pneumococcal triggering of epithelial-derived innate immunity. These differential epithelial cell responses may in part be due to differences in effects on pneumococcal metabolic pathways, activity of pneumolysin and hydrogen peroxide production, between the strains.

Despite almost identical colonisation profiles to WT, just a single bacterial gene mutation in metabolic genes revealed widespread and differing effects on pneumococcal-epithelial interactions and epithelial cell responses. Overall, our findings suggest that it is bacterial metabolism and virulence, but not pneumococcal load thresholds, that determine the epithelial host response. We propose this new paradigm has important implications for pneumococcal niche adaptation, transmission and transition towards disease.

GRAPHICAL ABSTRACT

Bacterial transcriptomics reveals profound changes in bacterial gene expression under stress, for which biosynthesis genes play a major role. During serum-induced stress and deletion of *proABC* or *fhs* genes, bacterial virulence factors such as ply and hydrogen peroxide regulator genes such as *spxB* were upregulated. Using a range of different cell culture models, all pneumococcal strains were able colonise and micro-invade epithelial cells. Bacterial load was not sufficient to account for the differences observed in epithelial gene expression, following infection with the pneumococcal strains. Epithelial cell responses were instead dependent upon bacterial adaptation profiles during nasopharyngeal colonisation. For example, deletion of the *fhs* gene induced a more intrinsic and epithelial repair response, enriching genes such as MAPK3/7, compared to 6B WT and deletion of the *proABC* gene which induced a more typical pro-inflammatory immune response, enriching genes such as RELA. The combination of host-pathogen interactions strengthens the link between bacterial metabolism and virulence which will ultimately influence the outcome of colonisation, transmission potential, transition to disease and generation of protective immunity.

INTRODUCTION

Adaptation to the host environment is crucial for successful colonisation of the upper respiratory tract by a range of human pathogens. This includes the ability to withstand different ambient

84 temperatures, overcome physical barriers such as mucus, evade epithelial cellular soluble mediators
85 such as antimicrobial peptides, compete with neighbouring polymicrobial communities and
86 compensate for nutrient restriction. *Streptococcus pneumoniae* (pneumococcus) is a common
87 commensal of the human upper respiratory tract (URT), but pneumococcal disease occurs following
88 translocation of the bacteria into the lungs which leads to pneumonia, into the blood which causes
89 sepsis and into the brain causing meningitis[1]. Indeed, among children under 5yrs, *S. pneumoniae* is
90 the leading cause of pneumonia deaths globally[2].

91 URT colonisation by the pneumococcus was previously thought to be restricted by the mucosal
92 epithelial barrier. However, using experimental human pneumococcal challenge (EHPC) of healthy
93 volunteers and well-characterised epithelial cell models, we have previously shown that colonisation
94 in health is characterised by epithelial surface microcolony formation and microinvasion (evidence
95 of epithelial invasion and transmigration without disease)[3]. We have previously shown that a *S.*
96 *pneumoniae* serotype 4 strain (TIGR4) invades Detroit 562 nasopharyngeal epithelial cells more
97 readily than serotype 6B and 23F strains, resulting in a marked pro-inflammatory epithelial
98 transcriptomic and cytokine profile[3]. Therefore, although an intracellular lifestyle during carriage may
99 allow the pneumococcus to avoid an adverse URT environment, an epithelial-innate immune
100 response is induced, leading us to propose that although the inflammatory response triggered by
101 epithelial microinvasion may result in bacterial clearance, it may also promote pneumococcal
102 transmission.

103

104 *S. pneumoniae* is highly variable with more than 100 serotypes as determined by polysaccharide
105 capsule, and more than 600 underlying global pneumococcal sequence clusters[4]. Pneumococcal
106 virulence, transmissibility and the potential to cause invasive disease are widely recognised as strain
107 dependent, influenced mainly by the polysaccharide capsule, and a wide range of subcapsular and
108 cytoplasmic proteins[5]. Bacterial cellular metabolism including carbohydrate, nucleotide and amino
109 acid biosynthesis have also been shown to play an important role in the outcome of host-
110 pneumococcal interactions[6-9].

111

112 Here we reveal that despite attenuation of disease following disruption of *S. pneumoniae* biosynthetic
113 genes, microinvasion was preserved as a feature of pneumococcal colonisation in both *in vitro* and
114 *in vivo* models. Crucially, we show that the differential downstream effects of microinvasion, including
115 the innate epithelial immune/ inflammatory response and cellular remodelling, are not simply
116 correlated to bacterial load, but more likely coupled to differing bacterial responses to stress.
117 Together our data highlight a disconnect between pneumococcal load and extent of epithelial cell
118 responses and instead suggests that the outcome of pneumococcal microinvasion of the epithelium
119 is intimately linked with bacterial metabolism and virulence characteristics expressed within the
120 epithelial niche. Our findings emphasise the complexity of the epithelial response to bacterial stress
121 during nasopharyngeal colonisation.

122

123

124 **RESULTS**

125 To explore the potential mechanisms that link bacterial metabolism to epithelial microinvasion and
126 inflammation during pneumococcal colonisation and avoid the confounders of different capsular or
127 genetic backgrounds, we have used isogenic mutants of *S. pneumoniae* serotype 6B which have
128 deletions of key biosynthesis genes; a γ-glutamyl phosphate reductase (*proA*), a γ-glutamyl kinase
129 (*proB*) and a pyrroline-5-carboxylate reductase s (*proC*), collectively referred to as *proABC*; a folate
130 tetrahydrofolate reductase (*fhs*); and then together with a deletion of pneumococcal iron acquisition
131 A (*piaA*)[10]. This double deletion ensures reversion does not occur during host experimental
132 challenge, in the EHPC model[11]. In a murine model, we have previously shown that the
133 Δ*proABC/piaA* and Δ*fhs/piaA* mutants effectively colonise but compared to the *S. pneumoniae*
134 serotype 6B wild type (WT), are attenuated in their ability to cause disease[12]. In the EHPC model
135 like the WT, both mutants retained the ability to colonise and induced IgG antibody production in
136 colonised individuals[11]. Therefore, we used these isogenic mutants, with a focus on the double

137 deleted strains, to retain comparability with the human infection experiments, to investigate the role
138 of microinvasion on induction of epithelial innate immunity.

139

140 **Deletions of *proABC* and *fhs* genes cause different broad-ranging effects on *S. pneumoniae***
141 **metabolism under stress conditions**

142

143 Given the potential complexity of the relationship between pneumococcal metabolism and virulence,
144 we first determined the wider impact of the *proABC* and *fhs* mutations on the pneumococcal in
145 response to human serum, to represent the physiological stress conditions found during infection.
146 The serotype 6B WT (strain BHN418) and its *proABC* and *fhs* isogenic mutant strains were grown
147 to mid-log phase in THY enriched media and then transferred to human serum for 60 minutes. We
148 found marked transcriptional differences between the WT and both mutants in response to serum
149 stress, associated with a more than three-fold increase in the number of upregulated genes for the
150 mutant strains compared to WT (data not shown). Genes differentially upregulated by the mutant
151 strains during serum stress included well-characterised pneumococcal virulence factors such as *ply*,
152 *nanA*, *psaA* and those regulating oxidative stress such as *lctO* (Supplementary Table 1).

153

154 Enrichment analysis of pathways of upregulated genes revealed that phosphotransferase systems,
155 amino nucleotide sugar, fructose and mannose and metabolic pathways were the most significantly
156 enriched pathways in the Δ*proABC* mutant under serum stress (Table 1). There was no disruption
157 in purine pathways or galactose metabolism. Enrichment pathway analysis for the Δ*fhs* mutant under
158 stress conditions revealed gene upregulation in competence, purine, pyruvate, metabolic pathways,
159 amino nucleotide sugar pathways and secondary metabolites (Table 1). Together these data
160 suggests that biosynthesis genes such as *proABC* or *fhs*, have widespread, but different effects on
161 metabolism which, during niche adaptation during colonisation, we postulate may be important
162 factors in the determination of host immunity.

163

164 ***S. pneumoniae* 6B with *proABC* or *fhs* mutations experimentally colonise humans with**
165 **enhanced microinvasion.**

166 We then tested whether the effects of these gene deletions on metabolism and subsequent growth
167 in sera also affected epithelial cell internalisation (microinvasion). Nasal curette samples from
168 healthy volunteers inoculated with the 6B WT or double mutant strains *(ΔproABC/piaA* or
169 *Δfhs/piaA*)[13] to were collected to investigate the extent of epithelial association and microinvasion,
170 (Figure 1A). A positive carrier was defined as colonisation at any time point (day 2 or day 6 post-
171 inoculation) within the study by microbiology culture (colony forming units, CFU counts) following a
172 nasal wash[3]. Mucosal cells collected by curettage were visualised by confocal microscopy for
173 analysis of direct interactions of the pneumococcal strains with the epithelium (Figure 1B).
174 Colonisation was achieved with all strains as analysed by microbiology and microscopy
175 (Supplemental Information Table 2). Unexpectedly, the day 6 post challenge samples revealed
176 greater microinvasion by both the *ΔproABC/piaA* or *Δfhs/piaA* strains compared to WT (Figure 1C),
177 with a higher microinvasive index (percentage of internalised bacteria / associated bacteria) as
178 shown in Figure 1D.

179

180 **Epithelial microinvasion is not dependent on bacterial load.**

181 We have previously demonstrated that the pattern of microinvasion and the subsequent epithelial
182 innate immune response to *S. pneumoniae* 6B seen in vitro with Detroit 562 cells, a human
183 nasopharyngeal carcinoma cell line, is similar to that seen in the EPHC model *in vivo*[3]. Therefore,
184 we used our Detroit 562 cell model to confirm the differences between the *ΔproABC/piaA* or
185 *Δfhs/piaA* strains compared to WT in microinvasion. We found that, as with the EHPC data, although
186 all strains still interacted with the epithelium forming surface colonies (Figure 2A), the isogenic
187 mutants associated less compared to 6B WT (Figure 2B), significantly so for *Δfhs/piaA* strain and
188 *Δfhs* single mutant strain. For all strains, microinvasion was observed with comparable absolute
189 numbers of internalised bacteria (Figure 2C), therefore resulting in a significantly elevated micro-
190 invasive index for the *ΔproABC/piaA* or *Δfhs/piaA* strains compared to WT (Figure 2D). Importantly,

191 for the single 6B mutant Δp*iaA* strain, epithelial association and microinvasion were not affected.
192 There were no significant differences in WT and mutant strain intracellular viability, with all strains
193 showing an approximately 50% reduction in intracellular CFU over 3 hours (Figure 1E). However,
194 despite the increased microinvasive index compared to WT, the single Δ*proABC* or Δ*fhs* and the
195 double Δ*proABC/piaA* or Δ*fhs/piaA* strains were impaired in their ability to transmigrate across the
196 epithelium (Figure 1F). This result is in keeping with previous evidence of disease attenuation in
197 murine models[12]. Similar trends for these strain interactions with epithelial cells were also observed
198 after one hour infection, suggesting bacterial replication does not play an important role in explaining
199 the differences observed between strains (Supplemental Information Figure 1).

200

201 Consistent with our previous findings for serotype 6B with Detroit 562 cells and Calu3 cells (a
202 bronchial epithelial cell line)[3], epithelial barrier function was not compromised after three hours of
203 infection; indeed, there was a tightening of the barrier evidenced by reduced FITC dextran diffusion
204 after pneumococcal exposure (Figure 2G). We found no evidence to suggest an impact on of
205 pneumococcal infection Junctional Adhesion Molecule A (JAM-A), Zonula-Occludens 1 (ZO-1),
206 Claudin 1 or Claudin 4 (Supplemental Figure 2). However, we did observe moderate increases in β
207 catenin expression following incubation with Δ*proABC/piaA* or Δ*fhs/piaA* strains, compared to WT
208 infected cells (Figure 2H, 2I). We detected a modest but statistically significant increase in cell death
209 after six hours, as measured by secretion of Lactate Dehydrogenase (LDH), following infection with
210 *S. pneumoniae* with all the strains compared to non-infected cells (Figure 2J).

211

212 ***S. pneumoniae* colonisation and microinvasion of primary human airway epithelium leads to**
213 **cellular remodelling**

214 To further explore the impact of microinvasion on epithelial biology in a more complex environment,
215 we cultured *S. pneumoniae* serotype 6B and the isogenic biosynthesis mutants with primary human
216 bronchial epithelial airway (NHBE-A) cells in air-liquid interface. We found that all strains associated
217 with epithelial cells (Figure 3A, top) and were also detected inside epithelial cells, enclosed within

218 vacuoles as detected by TEM (Figure 3A, bottom). To evaluate the differential effects on barrier
219 function, we assessed junctional protein expression and barrier integrity. As previously described[3],
220 6B WT and mutant strains co-localised with Junctional Adhesion Molecule A (JAM-A, Supplemental
221 Information Figure 3A, arrow), with no change in overall JAM-A expression. However, we did observe
222 an increase in Zonula Occludens 1 (ZO-1) intensity at the junctional membrane for cells infected with
223 the 6B WT strain (Supplementary Figure 3B), and a significant increase in the intensity of β catenin
224 staining for cells infected with to all strains but in particular, with the Δ*proABC/piaA* strain (Figure 3B,
225 3C). There were no adverse effects on barrier integrity, as measured by transepithelial electrical
226 resistance (Figure 3D), or cell death as measured by the release of lactate dehydrogenase (LDH,
227 Figure 3E) over the infection period.

228

229 When cultured in an air-liquid interface, NHBE cells differentiate into typical respiratory epithelium
230 cell types: Goblet, Clara, Basal and Ciliated cells (Figure 4A). Although we found no evidence to
231 suggest the pneumococcus preferentially colonised particular cell-types, pneumococci were
232 observed to be co-localised with mucus (mucin5ac positive, Figure 4C, arrows) and caught-up within
233 cilia (acetylated tubulin positive cells, Figure 4B and Supplemental Information Figure 4). Strikingly
234 however, while the cellular composition of the epithelial cultures exposed to the Δ*fhs/piaA* strain were
235 comparable in appearance to non-infected cells, exposure to the 6B WT and Δ*proABC/piaA* strains
236 resulted in an increased abundance of uteroglobin staining (found on Clara cells, Figure 4D). We
237 quantified confocal microscopy images to assess the abundance of differentiated cells following
238 infection with different strains. We found a significant increase in abundance of acetylated tubulin
239 expression following infection with the Δ*proABC/piaA* strain (Figure 4E, left graph), no differences in
240 the expression of mucin5ac following infection with any strain (Figure 4E, right graph), and an
241 increased expression of uteroglobin following exposure to Δ*fhs/piaA* strain (Figure 4F, left graph).
242 The latter also translated into a significant increase in uteroglobin staining within the epithelium
243 (Figure 5F, right graph).

244 Together, these findings show that the pneumococcal infection induces significant remodelling of the
245 epithelium.

246

247 **Microinvasion is not the sole determinant of the epithelial transcriptomic response to**
248 **pneumococcal colonisation.**

249 We have previously shown a broad range of host transcriptomic responses from Detroit 562 cells
250 exposed to different pneumococcal strains including 6B (BHN418)[3]. To assess whether the
251 enhanced microinvasion and the cellular remodelling observed with the 6B biosynthesis gene
252 mutants are part of a coordinated inflammatory response, we assessed epithelial transcriptomic
253 profiles following pneumococcal infection by RNAseq. Compared to non-infected cells, we found that
254 all strains upregulated 78 core epithelial genes related to cytokine signalling in immune system, NLR
255 signalling and GPCR ligand binding. 193 genes were upregulated by both the 6B WT and
256 Δ*proABC/piaA* strains, characterised by Rhodopsin-like receptors, GPCR ligand binding, cytokine
257 signalling in Immune system, signalling by Interleukins and Toll Receptor Cascades. Infection with
258 the Δ*fhs/piaA* strain resulted in a markedly different transcriptomic profile with modest upregulation
259 of 254 genes, characterised by antigen processing, proteasomal pathways, GTP hydrolysis, and
260 intracellular stress responses (Figure 5A). Focusing on the 20 topmost upregulated epithelial genes
261 revealed again that infection with 6B WT or Δ*proABC/piaA* strain induced a similar transcriptomic
262 profile which contrasted with that of Δ*fhs/piaA* strain which upregulated different epithelial genes at
263 a relatively low-level induction (Figure 5B).

264

265 Transcription factors (Figure 5C), cellular kinases (Figure 5D) and cytokines (Figure 5E)
266 bioinformatically predicted to regulate differentially expressed genes again revealed the greatest
267 differences following infection with Δ*fhs/piaA* strain, with diminished NFκB and MAPK activation
268 predicted compared to 6B WT and Δ*proABC/piaA* strain. Infection with Δ*fhs/piaA* strain induced a
269 more intrinsic and epithelial repair response which included TBK1, Raf1, JAK1 kinases and IL-1 and
270 IL-33 cytokine signalling. To explore the functional consequence of autocrine / paracrine cytokine
271 activity in infected Detroit 562 cells, we also assessed the expression of validated transcriptional
272 modules that reflect cytokine activity. This showed that 6B WT and Δ*proABC/piaA* strains induced

273 high levels of IL-1A, IL-1B and IL-6 gene expression responses (Figure 6F). Infection of primary
274 epithelial cells with the Δ*fhs/piaA* strain further supports our Detroit 562 cell data, where we observed
275 a unique differential gene expression profile compared to infection with 6B WT or Δ*proABC/piaA*
276 strains (Supplemental Information Figure 5).

277

278 **Deletion of *proABC* and *fhs* genes influence pneumococcal pneumolysin activity and**
279 **hydrogen peroxide production.**

280 The *S. pneumoniae* pore forming toxin pneumolysin can both activate and suppress the innate
281 immune response[14,15]. Pneumolysin also mediates the haemolytic activity characteristic of the
282 pneumococcus[16]. We therefore hypothesised that differential expression of pneumolysin among the
283 mutant strains may explain the differences in epithelial cell transcriptomes resulting from infection
284 with the WT and the isogenic mutant strains. Compared to 6B WT, we observed a significant increase
285 in pneumolysin gene expression by the Δ*proABC* and Δ*fhs* strains, following serum stress
286 (Supplemental Information, Table 1). We also observed significant increases in haemolytic activity
287 with the Δ*proABC* strain in a bioassay (Supplemental Figure 6). These potential differences in
288 pneumolysin expression may therefore partially explain differential effects on the epithelial
289 transcriptome and cellular remodelling following infection with the mutant strains compared to WT.

290

291 Hydrogen peroxide (H_2O_2) is released by *S. pneumoniae* during the stress of infection and is
292 regulated by enzymes encoded by such as s*pxB*, *spx* and *lctO* [17,18]. Both Δ*proABC* and Δ*fhs* strains
293 significantly increased expression of *spxB, lctO* and *adhE* transcripts when the bacteria were
294 cultured in serum-induced stress conditions, compared to WT (Supplementary Information Table 1).
295 We therefore postulated that differential expression of pneumococcal H_2O_2 may modulate epithelial
296 function during colonisation of the nasopharynx.

297

298 We next assessed whether H_2O_2 secretion from each strain could account for differences observed
299 in epithelial cell responses. Comparable levels of hydrogen peroxide were observed after one, three
300 and six hours of incubation, in the absence of epithelial cells (Figure 6A, dark grey bars). However,
301 in the presence of epithelial cells, less hydrogen peroxide levels were detected following infection
302 with Δ*fhs/piaA* strain compared to Δ*proABC/piaA* and WT at later time points (Figure 6A, light grey
303 bars). Of note, hydrogen peroxide secretion was significantly lower in the presence of epithelial cells
304 with all strains at one- and three-hours infection. This suggests either the presence of a suppression
305 factor derived from epithelial cells or induction of a niche adaptation response during colonisation.
306 Differences were not due to changes in bacterial load, as H_2O_2 levels remained comparable in the
307 presence or absence of epithelial cells for all strains (Figure 6B).

308

309 A growth rate function has been previously reported in the literature for *fhs* gene (Figure 6B)[19,20].
310 Adjustment for bacterial load reveals that Δ*fhs/piaA* pneumococci generate significantly more
311 hydrogen peroxide per bacterium, compared to 6B WT and Δ*proABC/piaA* strains (Figure 6C). These
312 responses could partially explain differences in epithelial transcriptomic profiles detected following
313 infection with the different strains.

314

315 To confirm whether the source of H_2O_2 was primarily from the pneumococcus and not the epithelial
316 cells, cells were incubated with the pneumococcal strains for 1hr and washed from non-adherent
317 bacteria. This removed bacteria from the supernatant so that only epithelial associated and bacteria
318 that have microinvaded remained. After a further 2 hours (total 3-hour timepoint) or 5 hours (total 6-
319 hour timepoint) incubation in fresh cell media, the amount of H_2O_2 was measured. Although
320 increased levels of H_2O_2 were detected following infection with all strains, compared to non-infected
321 cells (Supplemental Information Figure 7), levels were much lower compared to those obtained when
322 pneumococcal inoculum was present (Figure 6A).

323

324 Collectively, these data suggest that the major source of hydrogen peroxide was produced from
325 extracellular pneumococci but associated pneumococci to the epithelium and/or epithelial-derived
326 hydrogen peroxide also contributes.

327

328 **Differential Caspase Activity in Epithelial cells following infection with the pneumococcal**
329 **strains.**

330

331 Production of hydrogen peroxide by the pneumococcus influences the activity of the
332 inflammasome[21]. The NLRP3 inflammasome drives apoptosis via caspase 1 and regulates
333 pyroptosis via caspase 3/7 activity[21]. Therefore, we assessed caspase induction upon infection with
334 the different pneumococcal strains. We hypothesized that factors such as enhanced microinvasion,
335 pneumolysin activity and hydrogen peroxide production would enhance epithelial caspase activity.

336

337 Compared to non-infected cells, infection with 6B WT and Δ*proABC/piaA* strains led to a 1.5-fold
338 increase in epithelial caspase activity 3-hour post infection, with all strains inducing caspase activity
339 by 6hr post infection (Figure 7A, 7B, dark grey bars). To test which caspases were activated, we
340 incubated infected cell cultures with either a caspase 1 inhibitor (YVAD-CHO, Figure 7A, light grey
341 bars), a caspase 3/7 inhibitor (Z-VAD-FMK, Figure 7B, light grey bars), or specifically detected
342 caspase 8 activity (Figure 7C). The results show that at baseline, 8% of caspase activity was
343 attributable to caspase 1 (Figure 7A). However, upon infection, we detected an increase in caspase
344 activity in the presence of the caspase 1 inhibitor, suggesting activation of other caspases, in
345 particular following infection with Δ*fhs/piaA* and Δ*proABC/piaA* strains. This suggests differential
346 caspase induction following infection with different strains. Infection with primary epithelial cells also
347 revealed similar findings (Supplemental Information Figure 8).

348

349 Next, we measured caspase 3/7 activity in cells infected with the different pneumococcal strains. In
350 non-infected cells, 50% of caspase activity was attributable to caspase 3/7 activity, which was
351 unaffected following 3-hour pneumococcal infection (Figure 7B). However, following 6-hour
352 incubation with pneumococcal strains, caspase activity derived from epithelial cells infected with
353 Δ*proABC/piaA* strain was not caspase 3/7 driven (97% activity remaining after inhibition), compared
354 to Δfhs*/piaA* strain (73% activity remaining after inhibition).

355

356 Finally, we tested for caspase 8 activity and found significant activation following infection with 6B
357 WT and Δ*proABC/piaA* strains (Figure 7C).

358

359 Together, these data suggest that pneumococcal metabolism influences specific epithelial response
360 profiles that may affect induction of immunity.

361

362 **DISCUSSION**

363 There is considerable variation in the propensity *S. pneumoniae* strains to colonise the human host,
364 cause invasive disease and transmit to others[1]. We have previously proposed that epithelial
365 microinvasion and the subsequent inflammatory response may determine the outcome of
366 colonisation[3], and reported that epithelial association and microinvasion profiles differ between
367 pneumococcal strains with different capsular serotypes, and showed that these translated to unique
368 epithelial transcriptomic and protein expression profiles[3]. As well as the capsule, *S. pneumoniae*
369 factors affecting epithelial interactions or nasopharyngeal colonisation include multiple cell wall
370 adhesins[1] and pneumolysin[14]. In addition, multiple metabolic pathways likely to be required for
371 successful colonisation including those involved in DNA, protein, cell wall and fatty acid synthesis,
372 purine and pyrimidine metabolism, and oxidative phosphorylation[22]. The latter data indicates *S.*
373 *pneumoniae* metabolism, known to profoundly affect systemic infection[9,23,24], is also likely to have an
374 important role during the epithelial interactions that characterise colonisation.

375

376 To investigate this further, we have used well-characterised biosynthesis pathway isogenic mutants
377 attenuated for disease but not for carriage, to investigate whether *S. pneumoniae* metabolism affects
378 detailed interactions with respiratory epithelium[12]. *proABC* consists of three genes involved in proline
379 biosynthesis (ProABC) and *fhs* encodes the Fhs formate tetrahydrofolate synthetase which
380 catalyses the synthesis of N10 formyl tretrahydrofolate, crucial for carbon metabolism and purine
381 nucleotide biosynthesis in a number of bacterial species[19,25]. The function of the Fhs is thought to be
382 particularly relevant in hypoxic conditions[25,26]. We now demonstrate that alterations in pneumococcal
383 metabolism caused by deletion of *fhs* or *proABC* have profound effects on *S. pneumoniae*
384 transcriptome under stress conditions. This translates to effects on respiratory epithelium including
385 association, microinvasion, transmigration, and the subsequent epithelial inflammatory response,
386 cellular re-modelling and caspase activation. We implicate differences in pneumolysin and hydrogen
387 peroxide in the mediation of these epithelial responses to pneumococcal infection. Together these
388 data highlight the complex downstream effects of bacterial metabolism and indicate that epithelial
389 microinvasion by *S. pneumoniae* may result in a multitude of host cellular and bacterial outcomes
390 (Graphical Abstract). Indeed, adaptation to microinvasion by the pneumococcus may both facilitate
391 immune evasion and, as is typical of intracellular bacterial species such as *Listeria* and *Salmonella*,
392 ultimately trigger inflammation to mediate transmission[27,28].

393

394 Under stress, pneumococcal isogenic mutants upregulated virulence factors such as pneumolysin
395 and oxidative stress regulators that impacts on hydrogen peroxide secretion. This translated to an
396 enhanced microinvasive index, but attenuation of transmigration across, human nasopharyngeal
397 epithelium, highlighting the complex relationship between bacterial metabolism and virulence.

398

399 Using a well-characterised primary epithelial cell model[29], we found that *S. pneumoniae* interacts
400 with each of the constituent epithelial subtypes: clara cells (secretory, xenobiotic metabolic, and
401 progenitor cell functions), goblet cells (mucus production), ciliated cells (mucus and small particle

402 transport). The apparent downstream effects of infection with these biosynthesis mutants on
403 epithelial biology following microinvasion varied considerably. The intensity of β catenin, an
404 adherens junction protein, increased at the epithelial junctional membrane following infection with
405 the Δ*proABC/piaA* strain. Although there were no detectable effects on epithelial mucus production
406 following infection with the different strains, compared the WT, we saw an enrichment of staining for
407 acetylated tubulin (marker of ciliated cells) with Δ*proABC/piaA* exposure, and enrichment of staining
408 for uteroglobin (marker of clara cells) with Δ*fhs/piaA* exposure. We speculate that this cellular
409 remodelling could enhance barrier function or modulate permissiveness to bacterial microinvasion
410 and be important for bacterial clearance. Importantly, the differential epithelial effects following
411 infection with the different strains is striking, appearing not to relate to bacterial load and intracellular
412 survival potential, but instead more closely linked to pneumococcal-driven metabolic adaptations
413 that are not solely determined by capsule serotype.

414

415 Infection with either 6B WT or Δ*proABC/piaA* strain induced more typical innate inflammatory
416 pathways typical pneumococcal infection[3], including those related to cytokine/chemokines,
417 interleukins, Toll Like Receptor and NFκB signalling, together with apoptotic transcripts such as
418 FOXO3 and TP53. We also identified epithelial genes that were increased only following WT
419 infection included RNA degradation and O-linked glycosylation, compared to Δ*proABC/piaA* strain
420 infection that resulted in increased gene expression involved in wnt signalling (which may be linked
421 to the increase catenin expression we observed[30]), DNA sensing, RIG-I pathways and signal
422 transduction. In contrast, the Δ*fhs/piaA* strain appeared to activate an epithelial pro-survival and
423 adaptation profile which included JUN, SMARCA4, NFAT5, KLF6 and TCF4 genes involved in
424 homeostatic signalling and chromatin remodelling[31,32]. Together these illustrate the multifaceted
425 outcomes of epithelium microinvasion with the potential for either an inflammatory or more tolerant
426 response. Whether this translates to differences in the length of nasopharyngeal carriage,
427 invasiveness or clearance of the pneumococcal remains to be fully determined, but in the EHPC at
428 day 6, increased density of the Δ*fhs/piaA* strain was seen compared the other strains[11]. Ultimately,

429 these epithelial transcriptomic differences may also shape the adaptive immune response to
430 pneumococcal colonisation[13,33], which could also influence outcome.

431

432 *S. pneumoniae* is a catalase-negative, facultative anaerobe intrinsically resistant to hydrogen
433 peroxide (H_2O_2) which, particularly under conditions of aerobic growth, is produced endogenously
434 by pyruvate oxidase (*SpxB*) and acetate oxidase (*LctO*)[17,18,34]. Although, *SpxB* is not crucial for
435 pneumococcal disease (serotype 1 clones contain multiple mutations[35]), H_2O_2 production is a potent
436 virulence factor, limiting the growth of a variety of competing organisms in the upper respiratory tract,
437 inducing host cell endoplasmic reticulum stress, and is an intracellular signalling molecule that has
438 been shown to modulate inflammation, glycolytic flux, pyruvate metabolism, nucleotide biosynthesis,
439 and capsule biosynthesis[6,36]. We have shown that deletion of ProABC or Fhs genes impact on
440 pneumococcal oxidative stress regulation, which may contribute to epithelial remodelling, induction
441 of caspase and the epithelial transcriptomic response to infection. Hydrogen peroxide induces DNA
442 damage and apoptosis of the lung epithelium[21,37], but pneumococcal-derived hydrogen peroxide has
443 been shown to inhibit inflammasome activation[17].

444

445 *S. pneumoniae* is highly adapted to colonise the human host and be transmitted from person to
446 person. Invasive pneumococcal disease, particularly in it severest forms is largely a dead end. The
447 data presented here further support our hypothesis that epithelial microinvasion in healthy people is
448 common and mostly does not lead to disease. However, the subsequent epithelial-derived innate
449 responses to microinvasion are likely influenced by a range of bacterial metabolic and virulence
450 factors. Our findings highlight the broad-ranging effects of single gene mutations in pneumococcal
451 biosynthesis pathways which may in part, explain the complexity of the differences between even
452 seemingly closely related pneumococcal strains.

453

454 **METHODS**

455

456 **Bacteria**

457 The Streptococcus pneumoniae serotype 6B (strain BHN 418[38]) was a kind gift from Prof. Birgitta
458 Henriques Normark (Karolinska Institute). Δ*proABC/piaA* and Δ*fhs/piaA* mutant strains were
459 generated using overlap extension PCR as described by Ramos-Sevillano et al[12]. Stocks of bacteria
460 were stored at -80ºC when bacterial growth in Todd Hewitt Broth (THY) was 0.3 $O.D._{600nm}$. Aliquots
461 were defrosted, centrifuged at 8000g for eight minutes and resuspended in 1% Fetal Bovine Serum
462 (FBS, Gibco) in MEM media (Gibco) for infections. Approximately 10 bacteria were added for every
463 epithelial cell. Colony forming units (CFU) were counted by serial dilutions on horse blood agar plates
464 (EO Labs). Starting inoculums were not significantly different across strains for all assays.

465

466 **Bacterial RNA-Seq sample collection, sequencing and reads mapping**

467 Mutant pneumococcal strains (three biological replicates for each mutant) and 6B WT (three
468 biological replicates) were grown in THY to mid log phase and the pellets resuspended in THY and
469 undiluted human serum for 60mins. The culture was then pelleted, and total RNA extracted. Total
470 RNA from each library was ribo-depleted and sent for Illumina Next Seq Sequencing Pathogen
471 Genomics Unit (PGU), UCL. The quality of raw FASTQ reads was checked by FastQC v0.11.5,
472 Babraham Bioinformatics, UK [39] and visualised using multiQC v1.9[40]. Reads were trimmed using
473 Trimmomatic 0.39 [41]. Trimmed reads were also checked by FastQC and multiQC. Trimmed reads
474 were then mapped to KEGG annotated 6B genome sequence (670-6B, Accession: CP002176.1)
475 using bowtie2 with default settings [42]. Conversion into BAM files was performed using SAMtools [43].
476 Mapped reads were visualized in the Integrated Genome Browser (IGB) [44]. FeatureCounts v2.0.0
477 was used to summarize read counts for each annotated feature in the respective reference genomes
478 in multimapping mode (-M) [45].

479

480 **Differential gene expression analyses**

481 The generated count matrix was imported into R-studio (R v3.4.2) and normalization of counts and
482 differential gene expression analysis was performed by DESeq2 [46]. DESeq2 normalized libraries
483 were regularized log transformed for visualizing heatmaps and clustering. Differential gene
484 expression was performed on raw counts. Fold change shrinkage was implemented with the apeglm
485 package within DESeq2. Genes with a log2 fold change > 1.5 and false discovery rate (FDR) of <
486 0.05 were categorized as differentially expressed. KEGG pathway enrichment and module analysis
487 were performed on differentially regulated genes using over representation analysis (ORA)
488 implemented by clusterProfiler [47].

489

490 **Experimental Human Pneumococcal Carriage Model (EHPC)**

491 A full explanation of experimental design and selection criteria has been previously described[3].
492 Following written informed consent, healthy non-smoking adults between the ages of 18 – 59 were
493 inoculated with 80,000 CFU/nostril live strains of *S. pneumoniae*. Mucosal cells from the inferior
494 turbinate using a plastic Rhino-probe™ (curettage, Arlington Scientific) were collected prior to
495 inoculation, and days 2 and 6 post-inoculation. Samples were processed for confocal microscopy
496 analysis. Nasal wash samples were collected for CFU count analysis. There were no adverse events.

497

498 Ethical approval was given by NHS Research and Ethics Committee (REC)/Liverpool School of
499 Tropical Medicine (LSTM) REC, reference numbers: 18/NW/0481 and Human Tissue Authority
500 licensing number 12548.

501

502 **Primary Human Epithelial Cells**

503 Normal Human Primary Bronchial/Tracheal Epithelial Cells (NHBE-A, ATCC® PCS-300-010™) were
504 plated at $6x10^3$ cells/cm^2 on a layer of sub-lethally γ-irradiated (60 Gy) mouse embryonic fibroblasts
505 3T3-J2 cells (kind donation from Howard Green, Harvard Medical School, Boston[48]) with keratinocyte
506 culture medium cFAD (3:1 DMEM (Gibco) to Ham F-12 Nut Mix (Gibco), 10% FBS (HyClone, Sigma),
507 1% Penicillin-Streptomycin (100X, Sigma), 0.4 µg/mL Hydrocortisone (Calbiochem, USA), 5 µg/ml

508 Insulin (various), 10-10 Cholera Toxin (Sigma) and 2x10-9 Triodothyronine (Sigma)). Epithelial cells
509 were stimulated with 10 ng/mL human epidermal growth factor (hEGF, PeproTech, USA) on days 3
510 and 5. Cultures were grown at 37°C 6% CO_2 and sub-confluent cultures were trypsinised with 0.25%
511 Trypsin-EDTA (Sigma). For NHBE-A differentiation in Air Liquid Interface (ALI) culture, cells were
512 plated at a density of $6x10^4/cm^2$ on 1µm pore PET cell culture inserts (12 wells, Greiner). The insert
513 was supplemented with cFAD medium on the top and bottom. After 48 hours, medium was removed
514 from the top of the culture (exposure) and the culture was fed with fresh PneumaCult™ differentiation
515 Medium (Stemcell Technologies) from the bottom of the well every 2 days for 3 weeks, until cell
516 ciliation was observed. Antibiotics were removed from the medium and cells washed 24 hours before
517 infection experiments.

518

519 **Human Epithelial Cell Lines**

520 Human pharyngeal carcinoma Detroit 562 epithelial cells (ATCC_CCL-138) were grown in 10% FCS
521 in alpha MEM media (Gibco). For each set of experiments, cells were used within 5 passages. Cells
522 consistently tested PCR negative for mycoplasma (Cambridge Biosciences).

523

524 **Pneumococcal-epithelial cell co-culture**

525 For association and internalisation assays, confluent monolayers of Detroit 562 cells (typically day 7
526 - 8 post plating) cultured on 12 well plates (Corning), were exposed to *S. pneumoniae* (1 cell : 10
527 pneumococci) for three hours in 1% FCS alpha MEM (six-hour infection for HNBE-A cells in 1%
528 Pneumocult media without supplements)[3]. Cells washed three times in $HBSS^{+/+}$ before incubation in
529 1% saponin for 10 minutes at 37°C to lyse cells. Bacterial dilutions were plated on horse blood agar
530 for 16 hours and colony forming units counted. For internalisation quantification, 200µg/ml
531 gentamicin was added to the cells for one hour before incubation with saponin.

532

533 For transmigration assays, Detroit 562 cells were plated onto 3µm pore, PET Transwell Inserts
534 (ThermoFisher) typically for 10 days[3]. Media was changed to 1% FCS (250µl apical chamber, 1ml
535 basal chamber) one hour prior to infection experiments. 1mg/ml FITC-dextran (Sigma Aldrich) was

536 added to the apical chamber of selected inserts for permeability assays. Transepithelial Electrical
537 Resistance (TEER) was measured before and after infection using an EVOM2 (World Precision
538 Instruments). Bacteria were added to the cells for three hours during of which 50µl of basal media
539 was repeatedly removed to measure bacterial load by counting CFU/well. Permeability was recorded
540 using a FLUOstar Omega (BMG Labtech) at 488nm.
541
542 **Confocal Microscopy**
543 Sample processing was performed as previously described[3]. Briefly, mucosal cells from the EHPC
544 model were placed directly into 4% PFA and cytospun onto microscope slides. NHBE-A cells and
545 Detroit 562 cells cultured on transwell membranes were fixed in 4% PFA (Pierce, Methanol Free).
546 Cells were permeabilised with 0.2% Triton X-100 for 10 minutes, blocked for one hour in blocking
547 buffer (3% goat serum and 3% BSA in PBS (Sigma)) and incubated with pneumococcal antisera
548 Pool Q (SSI Diagnostica) for one hour. Wheat germ agglutinin conjugated to Rhodamine (Vector
549 Labs) was added along with goat-anti rabbit IgG conjugated to Alexa Fluor 488 for 45 minutes in
550 blocking buffer. Primary (used at 1:100) antibodies used for epithelial cell proteins can be found in
551 Supplemental Information Table 3. Secondary (used at 1:500) antibodies were either goat anti-
552 mouse or goat anti-rabbit – Alexa Fluor 555 or 546, ThermoFisher. Of note, for epithelial protein
553 antibodies raised in rabbit, no pneumococcal staining was possible and therefore pneumococci will
554 not visible on the images (uteroglobin). DAPI solution was added for 5 minutes and cells were
555 mounted with Aqua PolyMount (VWR International) and a coverslip on the microslide. Pneumococci
556 were recorded by manual scanning of the whole cytospin for the EHPC samples. More than three
557 fields of view were recorded for each bacterial strain for Detroit 562 cell infections, using inverted
558 Zeiss LSM (either 700 or 880) confocal microscopes. Images were processed with Zeiss LSM Image
559 Browser. Z stacks were recorded at 1µm intervals at either 40x oil or 63x oil objectives. Automated
560 image analysis was carried out using Cellprofiler[49].
561
562 **Electron Microscopy**

563 Preparation of Detroit 562 cells and NHBE-A cells was identical, and previously described[3]. Briefly,
564 cells cultured on transwells were fixed with 2% paraformaldehyde and 1.5% glutaraldehyde in 0.1 M
565 cacodylate buffer and post-fixed in 1% OsO4 / 1.5% K4Fe(CN)6 in 0.1 M cacodylate buffer pH7.3.
566 Samples were dehydrated in graded ethanol-water series and infiltrated with Agar 100 resin mix.
567 Ultra-thin sections were cut at 70-80 nm using a diamond knife on a Reichert ultracut microtome.
568 Sections were collected on 300 mesh copper grids and stained with lead citrate. For transmission
569 electron microscopy the samples were hardened at 60°c for 48 hours. The coverslip was removed,
570 and a representative area was selected. Ultra-thin sections were cut at 70-80 nm using a diamond
571 knife on a Reichert ultra-cut S microtome. Sections were collected on copper grids and stained with
572 lead citrate. Samples were viewed with a Joel 1010 transition electron microscope and the images
573 recorded using a Gatan Orius CCD camera.
574
575 **Pneumolysin activity**
576 Adapted from Kirkham et al[50]. Briefly, final concentration of 2% horse blood (EO Labs) solution was
577 prepared in phenol free alpha MEM (Life Technologies) and 100 µl added to wells of a 96 U-bottom
578 plate (Corning). 100 µl of bacterial solutions (containing progressively diluted bacteria) suspended
579 in phenol free alpha MEM were added to each 96 well. Saponin was used as a positive control for
580 lysis. Solutions were incubated for 30 minutes at 37°C before centrifugation at 1000g for one minute.
581 100 µl was transferred into a new 96 well plate and absorbance recorded at 540nm on a plate reader.
582
583 **Hydrogen Peroxide Assay**
584 Detroit 562 cells were cultured in white 96 well plates (Corning). NHBE-A cells were cultured in 12
585 well plates in Pneumocult media. Cells were incubated with H_2O_2 substrate and infected with strains
586 of *S. pneumoniae* for up to six hours according to manufacturers' instructions (ROS-Glo™ H_2O_2
587 Assay, Promega). ROS-Glo™ Detection solution was added to the cells and incubated for 20
588 minutes. For primary cells, supernatant was then transferred to a white 96 well plate. Luminescence
589 was read using a GloMax -Multi Detection System plate reader (Promega).
590
591 **Lactate Dehydrogenase Assay**

592 Detroit 562 cells and NHBE-A cells were cultured in 12 well plates and infected with pneumococcal
593 strains for six hours. Supernatant was centrifuged at 8000g for 8 minutes and pellet discarded.
594 Supernatant was transferred to a clear 96 well plate (Corning) and CytoTox 96® Reagent was added
595 for 30 minutes according to manufacturers' instructions (CytoTox 96® Non-Radioactive Cytotoxicity
596 Assay, Promega). After adding Stop Solution, absorbance was measured at 490nm using a plate
597 reader. % Cytotoxicity was calculated using the following equation: 100 x (LDH release – background
598 from media alone)/(max LDH release from positive control – background from media alone).
599

600 **Caspase assay**

601 Detroit 562 cells were cultured in white 96 well plates (Corning). NHBE-A cells were cultured in 12
602 well plates in Pneumocult media. Cells were infected with strains of *S. pneumoniae* for up to six
603 hours. Primary cell supernatant was transferred to a white 96 well plate. Samples were incubated
604 with Caspase-Glo® 1 Reagent, Caspase-Glo® 1 YVAD-CHO Reagent, Caspase-Glo® Z-VAD-FMK
605 Reagent or Caspase-Glo® 8 Reagent, for one hour and according to manufacturers' instructions
606 (Promega). Luminescence was read using a GloMax-Multi Detection System plate reader
607 (Promega).

608

609 **RNA samples and sequencing (RNA-Seq)**

610 RNA-Seq data was collected as previously described[3]. Confluent monolayers of Detroit 562 epithelial
611 cells were infected with *S. pneumoniae* strains for four hours before collection in RNALater. RNA
612 was extracted using a Qiagen RNAEasy micro kit and treated for DNA removal using a Qiagen Turbo
613 DNA-free kit. RNA quality was assessed and quantified using a BioAnalyser (Agilent 2100). Samples
614 were sequenced using Illumina Nextseq 500/550 High Output 75 cycle kit giving 15-20 million 41bp
615 paired-end reads per sample (Pathogens Genomic Unit, UCL).

616

617 **Data and code availability**

618 Source data are provided as a Source Data file. RNAseq data from the Detroit 562 cell infections is
619 publicly accessible through Zenodo with Accession (DOI:10.5281/zenodo.7997789).

620

621 **Statistics**

622 Each condition within each experiment was performed in duplicate or triplicate, and each experiment
623 was performed independently more than three times, unless stated otherwise. Error bars represent
624 SEM, unless stated otherwise. GraphPad Prism Version 10 was used for parametric (t-tests or
625 ANOVA) or non-parametric (Mann-Whitney or Kruskal-Wallis tests) analysis, which was based on
626 the Shapiro-Wilk normality test. Ad hoc tests were performed using Tukey's (for parametric data) or
627 Dunn's (for non-parametric data) multiple comparisons test. P values less than 0.05 were considered
628 significant.

629

630 **ACKNOWLEDGEMENTS**

631 This study was funded by a Postdoctoral Innovation Award from UCL to CMW, a Pump-Priming
632 Award and Enhancement Award from the Human Infection Challenge Network for Vaccine
633 Development (HIC-VAC), funded by the GCRF Networks in Vaccines Research and Development
634 which is co-funded by the MRC and BBSRC. This UK funded award is part of the EDCTP2
635 programme supported by the European Union. CMW and RSH are supported by the Medical
636 Research Council (grant MR/T016329/1). The authors would like to thank Prof. Peter Hermans
637 (Radboud University Medical Centre) for donating the 6B pneumococcal strain originally from Prof.
638 Birgitta Henriques-Normark (Karolinska Institute) and obtained directly from DF at LSTM. EHPC
639 sample collection was supported by the Medical Research Council (grant MR/M011569/1), Bill and
640 Melinda Gates Foundation (grant OPP1117728) awarded to DF and the National Institute for Health
641 Research (NIHR) Local Comprehensive Research Network. The authors also wish to thank the
642 EHPC Clinical Team at LSTM and all the volunteers. Confocal imaging facilities at LSTM were
643 funded by a Wellcome Trust Multi-User Equipment Grant (104936/Z/14/Z). Electron microscopy
644 processing and image capture was performed by Dr. Elizabeth Slavik-Smith in the Biosciences EM
645 facility at UCL. MC is supported by a Springboard to Independence grant (AirwayStasis) from the

646 French Government's Investissement d'Avenir program, the Laboratoire d'Excellence ''Integrative
647 Biology of Emerging Infectious Diseases" (ANR-10-LABX-62-IBEID) and the Chromatin and infection
648 unit headed by Melanie A. Hamon. RNA-Seq library preparation was undertaken at UCL through the
649 UCL/UCLH Biomedical Research Centre and MRC funded Pathogen Genomics Unit (PGU,
650 G0900950). All RNAseq data processing was completed by the PGU. Mahdad Noursadeghi is
651 supported by the Wellcome Trust and by NIHR Biomedical Research Centre Funding to University
652 College Hospitals NHS Foundation Trust and University College London. P.B. is supported by the
653 European Research Council (ERC-Stg No. 639429), the Rosetrees Trust (M362-F1; M553), the CF
654 Trust (SRC006;SRC020), the London Advanced Therapies - Research England (C2N-AT.006), the
655 MRC Confidence in Concept scheme (Award: MC_PC_17180), the Innovate UK (Smart grant
656 n.10005465), the Duchenne Parent Project (DPP) and the NIHR GOSH BRC. R.R. is supported by
657 Marie Skłodowska-Curie Individual Fellowships 896014. ERS and JSB are supported by MRC grant
658 R/N02687X/1 and Wellcome grant 221803/Z/20/Z. JSB is partially supported by the Department of
659 Health's National Institute of Health and Care Research Biomedical Research Centre funding to
660 UCLH. RSH is a NIHR Senior Investigator.

661

662 **AUTHOR CONTRIBUTIONS**: CMW conceived, funded, designed and conducted the study,
663 performed the experiments, acquired samples and processed data, and wrote the first draft of the
664 manuscript. GP analysed and interpreted the RNAseq data. MB analysed and interpreted the
665 bacterial transcriptomic data. RR cultured and differentiated primary epithelial cells. MC ran the
666 primary cell qPCR. ERS generated the mutant strains and bacterial transcriptomic data. JR collected
667 and processed EHPC samples. JAGA processed the RNA-Seq data. MW ran the image analysis.
668 PB and CJ provided investigator support. MN provided RNA-Seq analysis support. DF provided
669 investigator support and EHPC clinical samples. JSB generated the mutant strains, interpreted the
670 data and revised the manuscript. RSH provided investigator support, designed and interpreted the
671 data, revised the manuscript. All authors commented on and approved the manuscript.

672

673 **COMPETING INTERESTS:** The authors declare no competing interests.

674

675 **FIGURE LEGENDS**

676 **Table 1. Differentially expressed pathways from single isogenic mutants in human serum**
677 **compared to WT.** 55 genes were selected within competence pathways, amino acid metabolism,
678 virulence factors, oxidative stress pathways and other known genes important for colonisation, for
679 assessment of changes in gene expression following serum stress.

680

681 **Figure 1. Pneumococcal – epithelial interactions in the EHPC model**. (A) During colonisation,
682 pneumococci adhere to the epithelial cell surface (Association), internalise inside epithelial cells
683 (Microinvasion) and transmigrate across the mucosal barrier. Mucus – lime; pneumococci – teal;
684 intracellular vacuole – cream; epithelial cells– brown; nucleus – dark brown; cell junctions – pink. (B)
685 Representative microscopy images showing 6B association to the epithelium and mutant
686 microinvasion. Surface carbohydrates (red), nuclei (DAPI, blue), pneumococci (green). (C) Mucosal
687 curettage samples were collected at day 6 post-pneumococcal challenge. Percentage of bacteria
688 that were found by microscopy, on the surface (association) or inside (microinvasion) cells in the
689 EHPC model. Number of volunteers (n) in each group is indicated in brackets, along with the total
690 numbers of pneumococci (Spn) counted. (D) Micro-invasive index per volunteer, calculated from
691 microscopy counts, for each strain. P = 0.1701, Kruskal-Wallis.

692

693 **Figure 2**. **Strain association, microinvasion and transmigration of Detroit 562 cells.** Cells were
694 infected with *S. pneumoniae* for three hours and CFU counts recorded. (A) Representative confocal
695 microscopy images from 6 independent experiments with replicates, showing pneumococcal (green)
696 interactions with surface carbohydrates (red). (B) Association of pneumococcal strains to epithelial
697 cells. P = 0.0009 (Kruskal-Wallis), n = 6 with replicates. (C) Internalisation of strains into cells. P =
698 0.0219 (Kruskal-Wallis) N = 6 with replicates. (D) Microinvasive index is defined as the percentage
699 of internalised bacteria over all associated bacteria. P = 0.071 (Kruskal-Wallis) N = 6 with replicates.
700 (E) Pneumococcal viability inside epithelial cells after 3hr infection was assessed using a gentamicin

701 protection assay and refreshing the media for +1-+3hrs. n = 3 or 4 independent experiments with
702 replicates. Counts were normalised to microinvasion counts for each strain after 3 hours infection
703 and compared to 6B WT; +1hr P = 0.6517 (ANOVA), +2hr P = 0.1377 (ANOVA), +3hr P = 0.1183
704 (ANOVA). (F) Transmigration of pneumococcal strains in Detroit 562 cells after 3hrs infection. 6B
705 strains were added to the apical chamber of a transwell insert with a confluent monolayer of Detroit
706 562 cells. CFUs were recorded after 3hrs from the basal chamber, reflecting bacteria that had
707 transmigrated across the epithelium. N = 6 independent experiments with replicates. P < 0.001
708 (Kruskal-Wallis). (G) Cells cultured on transwell inserts were exposed to 6B strains for 3hrs and leak
709 to 4kDa FITC-Dextran was measured in the basal chamber by a fluorescent plate reader against a
710 standard. N = 4 with replicates. P <0.0001 compared to non-infected cells, and P = 0.0689 between
711 6B WT and mutant strains (Kruskal-Wallis). (H) Representative confocal microscopy images from 6
712 independent experiments with replicates, showing pneumococcal (green) interactions with β catenin
713 (red). Nuclear DAPI stain shown in blue. (I) Image quantification of integrated intensity of β catenin
714 normalised to non-infected cells, following infection with the different strains. N = 5 independent
715 experiments. ** P = 0.0034 (non-infected v infected), ** P = 0.0012 (6B v isogenic mutants), NS P =
716 0.0772 (non-infected v infected) Kruskal-Wallis. (J) Cell supernatant from infected cells was analysed
717 for lactate dehydrogenase secretion from the apical and basal chamber. N = 3 - 5 with replicates. P
718 = 0.046 compared to non-infected cells, and P = 0.5649 between 6B WT and mutant strains
719 (ANOVA).

720

721 **Figure 3. Effects on epithelial barrier from pneumococcal infection in HBE-A cells.** Cells were
722 cultured at ALI and infected with pneumococcal strains for 6hrs. (A) Top: Representative confocal
723 microscopy images from 4 independent experiments with replicates, showing pneumococcal (green)
724 association with the epithelium (red, surface carbohydrates; nuclei blue) at 6hr post infection.
725 Bottom: Representative transmission electron microscopy images from 2 independent experiments,
726 showing pneumococcal microinvasion examples of each strain (arrows), enclosed within a vacuole
727 after 4hr infection. (B) Representative confocal microscopy images from 4 independent experiments
728 with replicates, showing pneumococcal (green) interactions with junctional proteins (red) of (A) β

729 catenin. Colocalization of red and green appears yellow. Nuclei (blue). (C) Integrated intensity of β
730 catenin in pneumococcal negative or positive cells. P = >0.05, ANOVA. N = 4 independent
731 experiments. (D) Transepithelial electrical resistance (TEER) was recorded pre- and post- 6hr
732 infection to assess barrier integrity. N = 3 independent experiments with replicates. Average TEER
733 pre-infection was 466Ω.cm^2 (430-484 Ω.cm^2, P = 0.1458 ANOVA) and average TEER post-infection
734 was 545Ω.cm^2 (527-567 Ω.cm^2. P = 0.04744 ANOVA). Change in TEER comparing non-infected
735 cells to infected cells P = 0.6592, Kruskal-Wallis. Error bars represent SEM. (E) After infection,
736 supernatant was collected after 6hrs and analysed for lactate dehydrogenase secretion from the
737 apical and basal chamber. Non-infected v infected; P >0.05, ANOVA. N = 5-6 independent
738 experiments with replicates.

739

740 **Figure 4. Pneumococcal – epithelial interactions with primary human epithelial cells.** Cells
741 were cultured at ALI and infected with pneumococcal strains for 6hrs. (A) Representative scanning
742 electron microscopy images from 2 independent experiments, showing the surface of the epithelium.
743 Examples of differentiated epithelia (clara cells, goblet cells, ciliated cells) are shown for the
744 Δ*proABC/piaA* strain. Examples of pneumococci are highlighted by arrows. Representative confocal
745 microscopy images from 4 independent experiments with replicates for (B) ciliated cells (acetylated
746 tubulin, red), (C) goblet cells (mucin5ac, red, (arrows indicate co-localisation of mucin5ac with
747 pneumococci)), (D) clara cells (uteroglobin, red) shown after 6hr infection. Pneumococci (green),
748 nuclei (DAPI, blue), colocalization of red and green appears as yellow. (E) Integrated intensity of
749 acetylated tubulin and muc5ac in pneumococcal negative or positive cells. Acetylated tubulin neg P
750 = 0.2677, pos P = 0.017; mucin5ac neg P = 0.6852, pos P = 0.8510, ANOVA. N = 3 or 4 independent
751 experiments. (F) Integrated intensity of uteroglobin normalised to non-infected cells (left, P = 0.0115
752 non-infected v infected, Kruskal-Wallis) and percentage of clara positive cells following infection
753 (right, P = 0.0003 non-infected v strains, P = 0.0036 6B v mutant strains, Kruskal-Wallis). N = 3
754 independent experiments.

755

756 **Figure 5. Detroit 562 cell transcriptomic responses to pneumococcal strains.** Epithelial cells
757 were infected for four hours with pneumococcal strains and RNA extracted and processed for
758 RNAseq. 6B n = 11, PP n = 17, FP n = 14, non-infected n = 12, from 6 independent experiments.
759 (A) All significantly log2 fold change upregulated genes according to strain compared to non-infected
760 cells. Significance was defined as DEGs with a log2 fold change (logFC) of > 1.5 and false discovery
761 rate (FDR) of < 0.05. (B) Comparison of the top 20 most upregulated genes for each strain, compared
762 to non-infected cells. Upstream regulator analysis for (C) transcription factors, (D) kinases and (E)
763 cytokines. (F) The expression of gene modules is represented by the mean Log_2 TPM value of the
764 genes in each module.

765

766 **Figure 6. Hydrogen peroxide production from pneumococcal strains in the absence and**
767 **presence of Detroit 562 cells** (A) Supernatant from bacterial cultures without cells (dark grey) in
768 96 well white plates was assessed for production of reactive oxygen species, by luminescence and
769 compared to supernatant from bacterial-cell co-cultures (light grey). N = 5 independent experiments
770 with replicates. Without cells (dark grey), in comparison to 6B WT, 1hr P = 0.9087 (ANOVA), 3hr P
771 = 0.3310 (ANOVA), 6hr P = 0.7970 (ANOVA). With Detroit 562 cells (light grey), compared to non-
772 infected cells: 0hr P = 0.1437 (ANOVA), 3hr P <0.0001 (ANOVA), P = 0.0002 (Kruskal-Wallis).
773 Compared to 6B WT: 0hr P = 0.1399 (ANOVA), 3hr P = 0.006 (ANOVA), 6hr P = 0.0001 (ANOVA).
774 (B) Bacterial inoculum was measured by CFU counts collected from the supernatant and cultured
775 on blood agar plates for 16hr. n = 5 with replicates. Without cells, in comparison to 6B WT, 0hr P =
776 0.7652 (ANOVA), 1hr P = 0.0006 (Kruskal-Wallis), 3hr P = 0.0001 (ANOVA), P = 0.0279 (Kruskal-
777 Wallis). With Detroit 562 cells, in comparison to 6B WT, 0hr P = 0.4513 (ANOVA), 1hr P = 0.017
778 (ANOVA), 3hr P = 0.0002 (Kruskal-Wallis), 6hr P = 0.0103 (Kruskal-Wallis). (C) Fold change of
779 hydrogen peroxide production from the mutants compared to WT, normalised to the CFU counts.
780 Without cells (dark grey) 1h P = 0.0369 (ANOVA), 3hr P = 0.0087 (ANOVA), 6hr P = 0.0209 (Kruskal-
781 Wallis). With Detroit 562 cells (light grey), 1h P = 0.2170 (ANOVA), 3hr P = 0.0281 (ANOVA), 6hr P
782 = 0.0243 (Kruskal-Wallis). Δ*pp is* Δ*proABC/piaA* strain and Δ*fp* is Δ*fhs/piaA* strain.

783

784 **Figure 7. Effects of pneumococcal infection caspase secretion in Detroit 562 cells.** Caspase
785 activity was assessed by luminescence, following infection with pneumococcal strains. (A) Caspase
786 1 activity was determined following incubation with the specific inhibitor YVAD-CHO. N = 6 with
787 replicates. In comparison to non-infected cells, 3hr caspase P = 0.0297; caspase+YVAD-CHO
788 inhibitor P = 0.0479 and, in comparison to 6B WT, 3hr caspase P = 0.0173; caspase+YVAD-CHO
789 inhibitor P = 0.5725 (Kruskal-Wallis). In comparison to non-infected cells, 6hr caspase P = 0.39;
790 caspase+YVAD-CHO inhibitor P = 0.3604 and, in comparison to 6B WT, 6hr caspase P = 0.6226;
791 caspase+YVAD-CHO inhibitor P = 0.5386 (Kruskal-Wallis). (B) Caspase 3/7 activity was determined
792 following incubation with the specific inhibitor Z-VAD-FMK. N = 4 with replicates. In comparison to
793 non-infected cells, 3hr caspase P = 0.0001; caspase+Z-VAD-FMK inhibitor P = 0.0165 and, in
794 comparison to 6B WT, 3hr caspase P = 0.0036; caspase+ Z-VAD-FMK inhibitor P = 0.0036 (Kruskal-
795 Wallis). In comparison to non-infected cells, 6hr caspase P = 0.0022; caspase+ Z-VAD-FMK inhibitor
796 P = 0.0005 and, in comparison to 6B WT, 6hr caspase P = 0.0215; caspase+ Z-VAD-FMK inhibitor
797 P = 0.0012 (Kruskal-Wallis). (C) Caspase 8 activity was assessed following infection with
798 pneumococcal strains. N = 3 with replicates. In comparison to non-infected cells, 6hr P = 0.0015
799 (ANOVA) and, in comparison to 6B WT, P = 0.0172 (ANOVA).

800

801

802 **REFERENCES**

803 1 Weiser, J. N., Ferreira, D. M. & Paton, J. C. Streptococcus pneumoniae: transmission, colonization and
804 invasion. *Nat Rev Microbiol* **16**, 355-367, doi:10.1038/s41579-018-0001-8 (2018).
805 2 O'Brien, K. L. *et al.* Burden of disease caused by Streptococcus pneumoniae in children younger than
806 5 years: global estimates. *Lancet* **374**, 893-902, doi:10.1016/S0140-6736(09)61204-6 (2009).
807 3 Weight, C. M. *et al.* Microinvasion by Streptococcus pneumoniae induces epithelial innate immunity
808 during colonisation at the human mucosal surface. *Nat Commun* **10**, 3060, doi:10.1038/s41467-019-
809 11005-2 (2019).
810 4 Gladstone, R. A. *et al.* International genomic definition of pneumococcal lineages, to contextualise
811 disease, antibiotic resistance and vaccine impact. *EBioMedicine* **43**, 338-346,
812 doi:10.1016/j.ebiom.2019.04.021 (2019).
813 5 Amin-Chowdhury, Z. *et al.* Characteristics of Invasive Pneumococcal Disease Caused by Emerging
814 Serotypes After the Introduction of the 13-Valent Pneumococcal Conjugate Vaccine in England: A
815 Prospective Observational Cohort Study, 2014-2018. *Clin Infect Dis* **71**, e235-e243,
816 doi:10.1093/cid/ciaa043 (2020).

817 6 Echlin, H., Frank, M., Rock, C. & Rosch, J. W. Role of the pyruvate metabolic network on carbohydrate
818 metabolism and virulence in Streptococcus pneumoniae. *Mol Microbiol* **114**, 536-552,
819 doi:10.1111/mmi.14557 (2020).
820 7 Hartel, T. *et al.* Characterization of central carbon metabolism of Streptococcus pneumoniae by
821 isotopologue profiling. *J Biol Chem* **287**, 4260-4274, doi:10.1074/jbc.M111.304311 (2012).
822 8 Henriques-Normark, B. & Tuomanen, E. I. The pneumococcus: epidemiology, microbiology, and
823 pathogenesis. *Cold Spring Harb Perspect Med* **3**, doi:10.1101/cshperspect.a010215 (2013).
824 9 Kohler, S., Voss, F., Gomez Mejia, A., Brown, J. S. & Hammerschmidt, S. Pneumococcal lipoproteins
825 involved in bacterial fitness, virulence, and immune evasion. *FEBS Lett* **590**, 3820-3839,
826 doi:10.1002/1873-3468.12352 (2016).
827 10 Brown, J. S., Gilliland, S. M. & Holden, D. W. A Streptococcus pneumoniae pathogenicity island
828 encoding an ABC transporter involved in iron uptake and virulence. *Mol Microbiol* **40**, 572-585,
829 doi:10.1046/j.1365-2958.2001.02414.x (2001).
830 11 Hill H, M. E., Nikolaou E, Blizard A, Pojar S, Howard A, Hyder-Wright A, Devin J, Reiné J, Robinson R,
831 Solórzano C, Jochems S, Kenny-Nyazika T, Ramos-Sevillano E, Weight CM, Myerscough C, McLennan
832 D, MortonB , Gibbons E, Farrar M, Randles V, Burhan H, Chen T, Shandling AD, Campo JJ, Heyderman
833 RS, Gordon SB, Brown JS, Collins AM, Ferreira DM. A Randomised Controlled Trial of Nasal
834 Immunisation with Live Virulence Attenuated Streptococcus pneumoniae Strains using Human
835 Infection Challenge. *Medrxiv*, doi:https://doi.org/10.1101/2023.04.14.23288224 (2023).
836 12 Ramos-Sevillano, E. *et al.* Preclinical Development of Virulence Attenuated Streptococcus
837 pneumoniae Strains Able to Enhance Protective Immunity Against Pneumococcal Infection. *Am J*
838 *Respir Crit Care Med*, doi:10.1164/rccm.202011-4161LE (2020).
839 13 Ferreira, D. M. *et al.* Controlled human infection and rechallenge with Streptococcus pneumoniae
840 reveals the protective efficacy of carriage in healthy adults. *Am J Respir Crit Care Med* **187**, 855-864,
841 doi:10.1164/rccm.201212-2277OC (2013).
842 14 Zafar, M. A., Wang, Y., Hamaguchi, S. & Weiser, J. N. Host-to-Host Transmission of Streptococcus
843 pneumoniae Is Driven by Its Inflammatory Toxin, Pneumolysin. *Cell Host Microbe* **21**, 73-83,
844 doi:10.1016/j.chom.2016.12.005 (2017).
845 15 Periselneris, J. *et al.* Pneumolysin suppresses the initial macrophage pro-inflammatory response to
846 Streptococcus pneumoniae. *Immunology* **167**, 413-427, doi:10.1111/imm.13546 (2022).
847 16 Terra, V. S., Plumptre, C. D., Wall, E. C., Brown, J. S. & Wren, B. W. Construction of a pneumolysin
848 deficient mutant in streptococcus pneumoniae serotype 1 strain 519/43 and phenotypic
849 characterisation. *Microb Pathog* **141**, 103999, doi:10.1016/j.micpath.2020.103999 (2020).
850 17 Erttmann, S. F. & Gekara, N. O. Hydrogen peroxide release by bacteria suppresses inflammasome-
851 dependent innate immunity. *Nat Commun* **10**, 3493, doi:10.1038/s41467-019-11169-x (2019).
852 18 Alibayov, B. *et al.* Oxidative Reactions Catalyzed by Hydrogen Peroxide Produced by Streptococcus
853 pneumoniae and Other Streptococci Cause the Release and Degradation of Heme from Hemoglobin.
854 *Infect Immun* **90**, e0047122, doi:10.1128/iai.00471-22 (2022).
855 19 Crowley, P. J., Gutierrez, J. A., Hillman, J. D. & Bleiweis, A. S. Genetic and physiologic analysis of a
856 formyl-tetrahydrofolate synthetase mutant of Streptococcus mutans. *J Bacteriol* **179**, 1563-1572,
857 doi:10.1128/jb.179.5.1563-1572.1997 (1997).
858 20 Mahdi, L. K., Wang, H., Van der Hoek, M. B., Paton, J. C. & Ogunniyi, A. D. Identification of a novel
859 pneumococcal vaccine antigen preferentially expressed during meningitis in mice. *J Clin Invest* **122**,
860 2208-2220, doi:10.1172/JCI45850 (2012).
861 21 Surabhi, S. *et al.* Hydrogen Peroxide Is Crucial for NLRP3 Inflammasome-Mediated IL-1beta
862 Production and Cell Death in Pneumococcal Infections of Bronchial Epithelial Cells. *J Innate Immun*
863 **14**, 192-206, doi:10.1159/000517855 (2022).
864 22 van Opijnen, T. & Camilli, A. A fine scale phenotype-genotype virulence map of a bacterial pathogen.
865 *Genome Res* **22**, 2541-2551, doi:10.1101/gr.137430.112 (2012).
866 23 Basavanna, S. *et al.* The effects of methionine acquisition and synthesis on Streptococcus
867 pneumoniae growth and virulence. *PLoS One* **8**, e49638, doi:10.1371/journal.pone.0049638 (2013).
868 24 Gomez-Mejia, A. *et al.* Pneumococcal Metabolic Adaptation and Colonization Are Regulated by the
869 Two-Component Regulatory System 08. *mSphere* **3**, doi:10.1128/mSphere.00165-18 (2018).

870 25 Sah, S., Aluri, S., Rex, K. & Varshney, U. One-carbon metabolic pathway rewiring in Escherichia coli
871 reveals an evolutionary advantage of 10-formyltetrahydrofolate synthetase (Fhs) in survival under
872 hypoxia. *J Bacteriol* **197**, 717-726, doi:10.1128/JB.02365-14 (2015).
873 26 Aluri, S., Rex, K. & Varshney, U. Simultaneous presence of fhs and purT genes is disadvantageous for
874 the fitness of Escherichia coli growth. *FEMS Microbiol Lett* **362**, doi:10.1093/femsle/fnv101 (2015).
875 27 Galan, J. E. Salmonella Typhimurium and inflammation: a pathogen-centric affair. *Nat Rev Microbiol*
876 **19**, 716-725, doi:10.1038/s41579-021-00561-4 (2021).
877 28 Li, G. *et al.* Morin inhibits Listeria monocytogenes virulence in vivo and in vitro by targeting
878 listeriolysin O and inflammation. *BMC Microbiol* **20**, 112, doi:10.1186/s12866-020-01807-6 (2020).
879 29 Travaglini, K. J. *et al.* A molecular cell atlas of the human lung from single-cell RNA sequencing. *Nature*
880 **587**, 619-625, doi:10.1038/s41586-020-2922-4 (2020).
881 30 Liu, J. *et al.* Wnt/beta-catenin signalling: function, biological mechanisms, and therapeutic
882 opportunities. *Signal Transduct Target Ther* **7**, 3, doi:10.1038/s41392-021-00762-6 (2022).
883 31 Herta, T. *et al.* DNA-release by Streptococcus pneumoniae autolysin LytA induced Krueppel-like
884 factor 4 expression in macrophages. *Sci Rep* **8**, 5723, doi:10.1038/s41598-018-24152-1 (2018).
885 32 Barutcu, A. R. *et al.* SMARCA4 regulates gene expression and higher-order chromatin structure in
886 proliferating mammary epithelial cells. *Genome Res* **26**, 1188-1201, doi:10.1101/gr.201624.115
887 (2016).
888 33 Wilson, R. *et al.* Protection against Streptococcus pneumoniae lung infection after nasopharyngeal
889 colonization requires both humoral and cellular immune responses. *Mucosal Immunol* **8**, 627-639,
890 doi:10.1038/mi.2014.95 (2015).
891 34 Spellerberg, B. *et al.* Pyruvate oxidase, as a determinant of virulence in Streptococcus pneumoniae.
892 *Mol Microbiol* **19**, 803-813, doi:10.1046/j.1365-2958.1996.425954.x (1996).
893 35 Syk, A. *et al.* Emergence of hypervirulent mutants resistant to early clearance during systemic
894 serotype 1 pneumococcal infection in mice and humans. *J Infect Dis* **210**, 4-13,
895 doi:10.1093/infdis/jiu038 (2014).
896 36 Pericone, C. D., Overweg, K., Hermans, P. W. & Weiser, J. N. Inhibitory and bactericidal effects of
897 hydrogen peroxide production by Streptococcus pneumoniae on other inhabitants of the upper
898 respiratory tract. *Infect Immun* **68**, 3990-3997, doi:10.1128/IAI.68.7.3990-3997.2000 (2000).
899 37 Loose, M. *et al.* Pneumococcal hydrogen peroxide-induced stress signaling regulates inflammatory
900 genes. *J Infect Dis* **211**, 306-316, doi:10.1093/infdis/jiu428 (2015).
901 38 Browall, S. *et al.* Intraclonal variations among Streptococcus pneumoniae isolates influence the
902 likelihood of invasive disease in children. *J Infect Dis* **209**, 377-388, doi:10.1093/infdis/jit481 (2014).
903 39 S., A. FastQC: a quality control tool for high throughput sequence data. (2010).
904 40 Ewels, P., Magnusson, M., Lundin, S. & Kaller, M. MultiQC: summarize analysis results for multiple
905 tools and samples in a single report. *Bioinformatics* **32**, 3047-3048,
906 doi:10.1093/bioinformatics/btw354 (2016).
907 41 Bolger, A. M., Lohse, M. & Usadel, B. Trimmomatic: a flexible trimmer for Illumina sequence data.
908 *Bioinformatics* **30**, 2114-2120, doi:10.1093/bioinformatics/btu170 (2014).
909 42 Langmead, B. & Salzberg, S. L. Fast gapped-read alignment with Bowtie 2. *Nat Methods* **9**, 357-359,
910 doi:10.1038/nmeth.1923 (2012).
911 43 Li, H. *et al.* The Sequence Alignment/Map format and SAMtools. *Bioinformatics* **25**, 2078-2079,
912 doi:10.1093/bioinformatics/btp352 (2009).
913 44 Nicol, J. W., Helt, G. A., Blanchard, S. G., Jr., Raja, A. & Loraine, A. E. The Integrated Genome Browser:
914 free software for distribution and exploration of genome-scale datasets. *Bioinformatics* **25**, 2730-
915 2731, doi:10.1093/bioinformatics/btp472 (2009).
916 45 Liao, Y., Smyth, G. K. & Shi, W. featureCounts: an efficient general purpose program for assigning
917 sequence reads to genomic features. *Bioinformatics* **30**, 923-930, doi:10.1093/bioinformatics/btt656
918 (2014).
919 46 Love, M. I., Huber, W. & Anders, S. Moderated estimation of fold change and dispersion for RNA-seq
920 data with DESeq2. *Genome Biol* **15**, 550, doi:10.1186/s13059-014-0550-8 (2014).
921 47 Yu, G., Wang, L. G., Han, Y. & He, Q. Y. clusterProfiler: an R package for comparing biological themes
922 among gene clusters. *OMICS* **16**, 284-287, doi:10.1089/omi.2011.0118 (2012).

923 48 Rheinwald, J. G. & Green, H. Serial cultivation of strains of human epidermal keratinocytes: the
924 formation of keratinizing colonies from single cells. *Cell* **6**, 331-343, doi:10.1016/s0092-
925 8674(75)80001-8 (1975).
926 49 Carpenter, A. E. *et al.* CellProfiler: image analysis software for identifying and quantifying cell
927 phenotypes. *Genome Biol* **7**, R100, doi:10.1186/gb-2006-7-10-r100 (2006).
928 50 Kirkham, L. A. *et al.* Construction and immunological characterization of a novel nontoxic protective
929 pneumolysin mutant for use in future pneumococcal vaccines. *Infect Immun* **74**, 586-593,
930 doi:10.1128/IAI.74.1.586-593.2006 (2006).

931

Table 1

Pathway	GeneRatio	P-adjust	qvalue
Δ*fhs* vs. WT			
Fatty acid metabolism/biosynthesis	10/57	1.08E-09	6.49E-10
Biosynthesis of secondary metabolites	26/57	2.09E-04	1.26E-04
Purine metabolism	10/57	1.34E-03	8.06E-04
Quorum sensing	11/57	3.20E-03	1.92E-03
Pantothenate and CoA biosynthesis	5/57	3.59E-03	2.16E-03
beta-Lactam resistance	5/57	7.59E-03	4.57E-03
Propanoate metabolism	4/57	1.51E-02	9.09E-03
2-Oxocarboxylic acid metabolism	4/57	1.51E-02	9.09E-03
Metabolic pathways	40/57	1.94E-02	1.16E-02
Amino sugar and nucleotide sugar metabolism	7/57	4.22E-02	2.54E-02
Pyruvate metabolism	5/57	4.31E-02	2.59E-02
Δ*proABC* vs. WT			
Fatty acid metabolism/biosynthesis	10/71	1.17E-08	8.94E-09
Galactose metabolism	12/71	1.25E-04	2.47E-08
Phosphotransferase system (PTS)	13/71	2.54E-03	1.93E-03
Amino sugar and nucleotide sugar metabolism	9/71	2.89E-02	2.20E-02

Figure 1

A

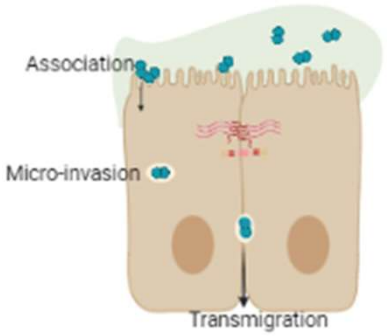

B

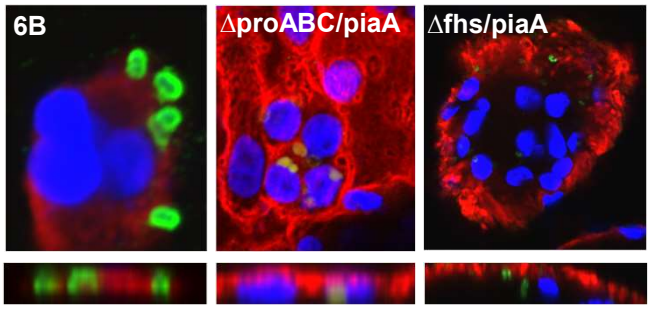

C

	Day 6 post-challenge	
	Association (%)	**Micro-invasion (%)**
6B	87.8 (n11, 43spn)	12.2 (n11, 6spn)
ΔproABC/piaA	59.3 (n11, 16spn)	40.7 (n11, 11spn)
Δfhs/piaA	48.7 (n5, 57spn)	51.3 (n5, 60spn)

D

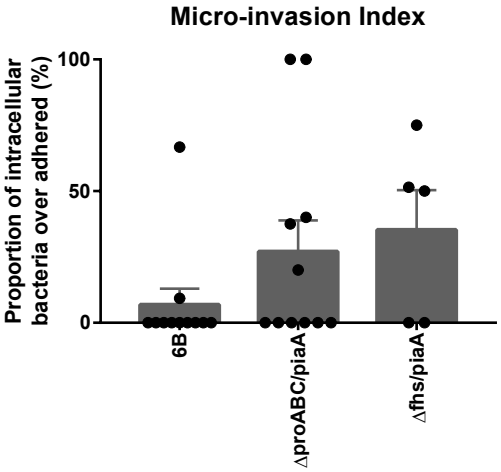

Figure 2

A

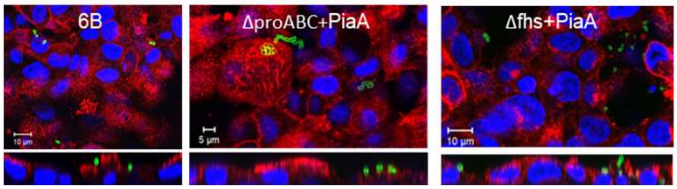

B

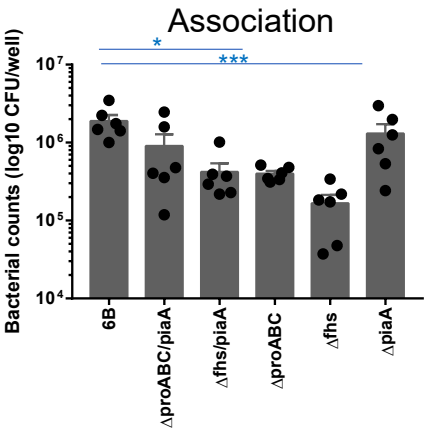

C

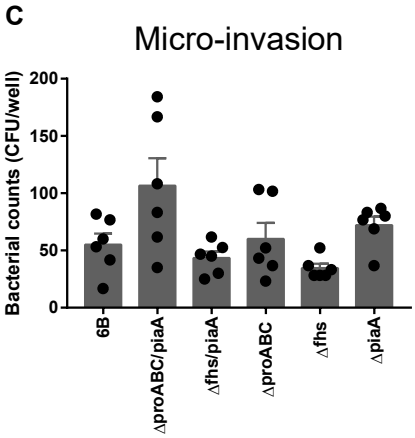

D

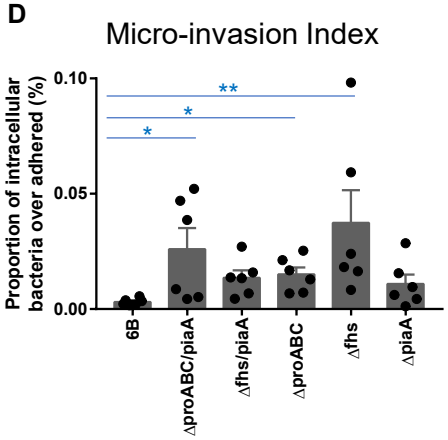

E

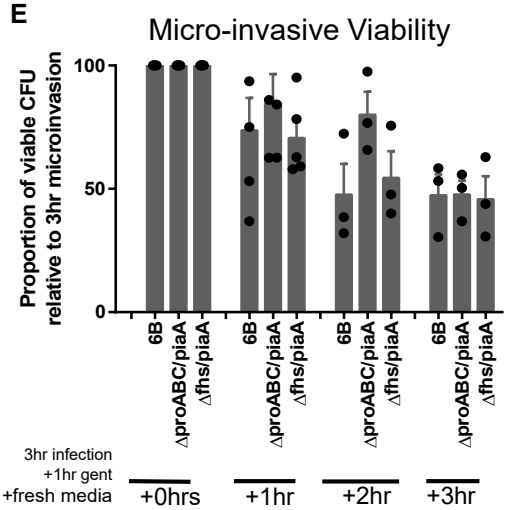

F

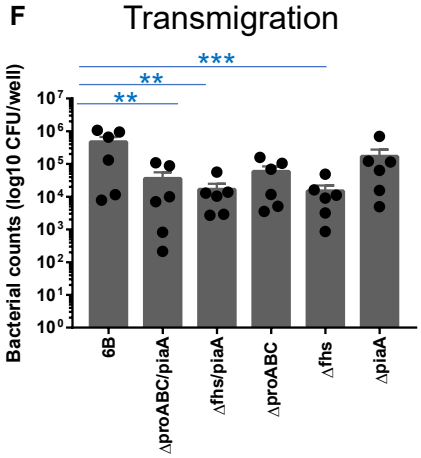

G

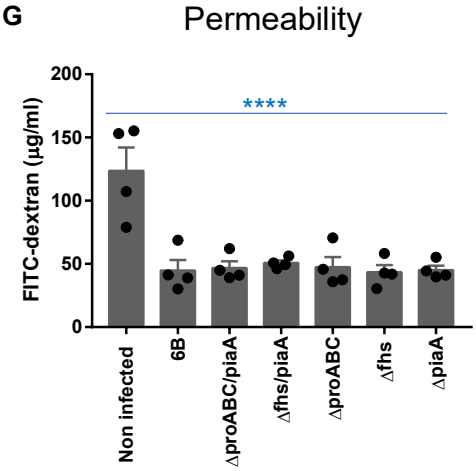

H

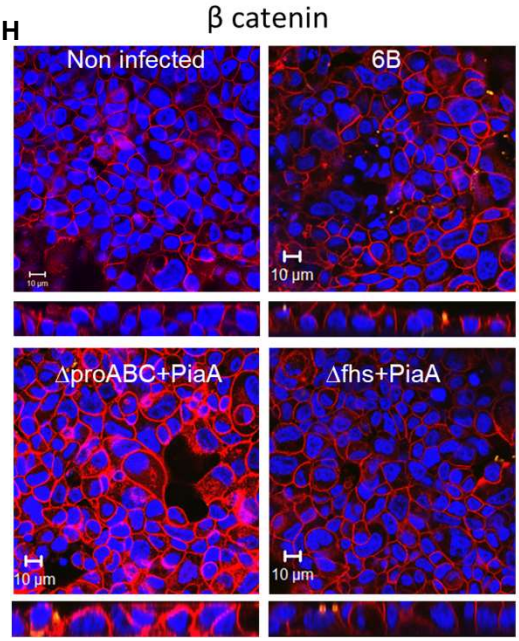

I

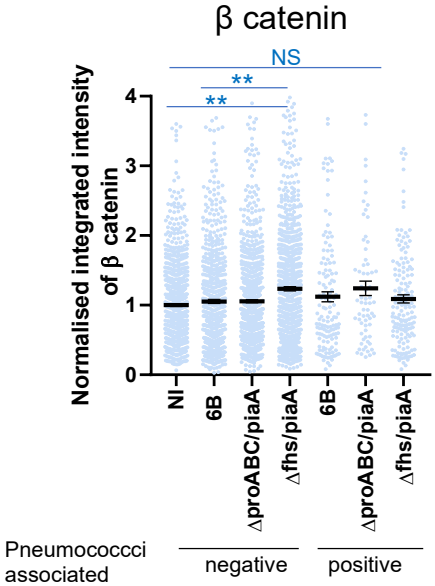

J

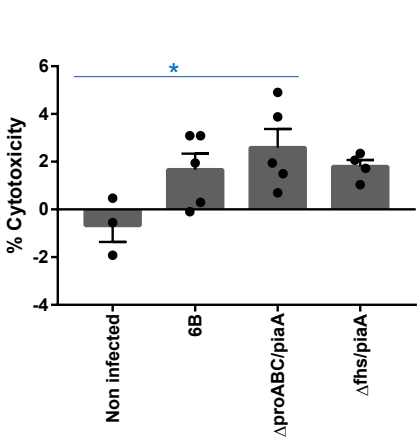

Figure 3

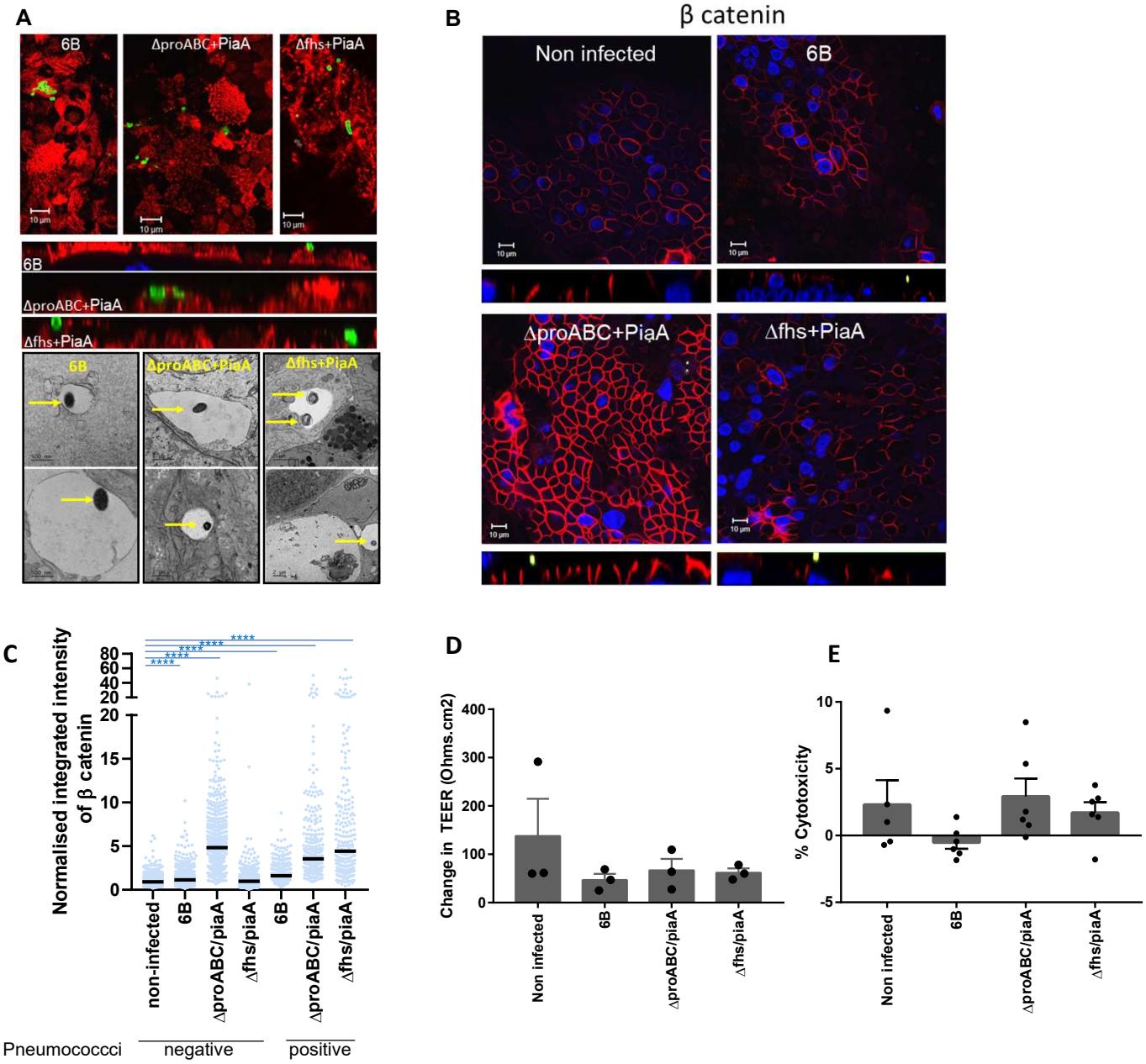
A
6B
ΔproABC+PiaA
Δfhs+PiaA
B
β catenin
Non infected
6B
ΔproABC+PiaA
Δfhs+PiaA
C
Normalised integrated intensity of β catenin
non-infected
6B
ΔproABC/piaA
Δfhs/piaA
Pneumococci
negative
positive
D
Change in TEER (Ohms.cm2)
Non infected
6B
ΔproABC/piaA
Δfhs/piaA
E
% Cytotoxicity
Non infected
6B
ΔproABC/piaA
Δfhs/piaA

Figure 4

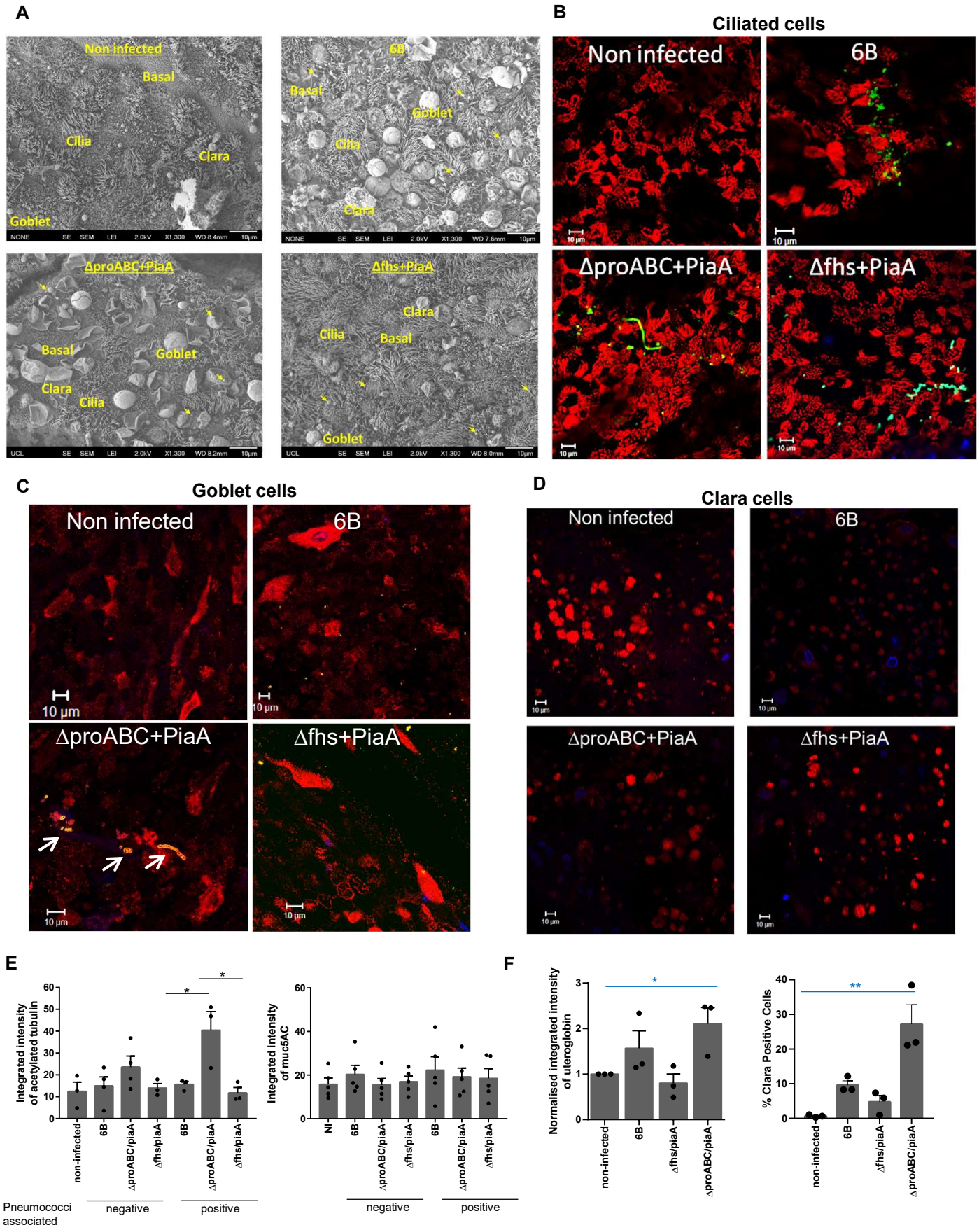
A
Non infected
Basal
Cilia
Clara
Goblet
6B
ΔproABC+PiaA
Δfhs+PiaA
B
Ciliated cells
Non infected
6B
ΔproABC+PiaA
Δfhs+PiaA
10 µm
C
Goblet cells
Non infected
6B
ΔproABC+PiaA
Δfhs+PiaA
D
Clara cells
Non infected
6B
ΔproABC+PiaA
Δfhs+PiaA
E
Integrated intensity of acetylated tubulin
non-infected
6B
ΔproABC/piaA
Δfhs/piaA
Pneumococci associated
negative
positive
Integrated intensity of muc5AC
NI
F
Normalised integrated intensity of uteroglobin
% Clara Positive Cells

Figure 5

A

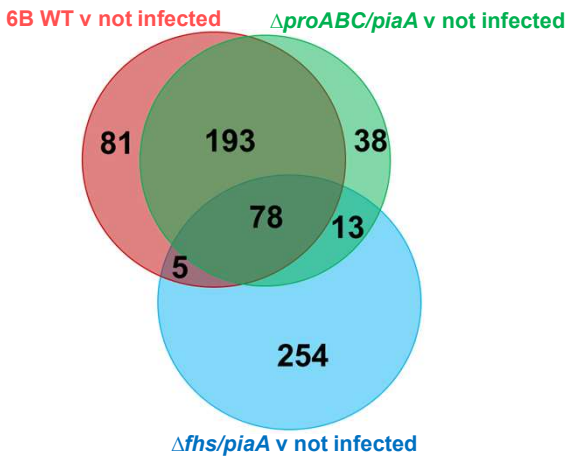

B

log2foldchange	6B	ΔproABC/piaA	Δfhs/piaA
Upregulated genes			
AC256236.1	32.9	25.5	0.0
AC022149.1	30.2	27.6	0.0
Z84488.2	29.1	21.6	0.0
MUC21	25.8	29.0	0.0
VASN	20.9	0.0	0.0
BRD2	18.4	24.7	0.0
AC012254.2	18.2	13.8	0.0
CTAGE4	18.1	0.0	0.0
MICE	17.1	20.3	0.0
AC107075.1	10.1	0.0	0.0
CSNK2B	0.0	20.2	0.0
MTRNR2L6	0.0	19.4	15.8
LSM2	0.0	17.1	0.0
ALOX5	0.0	0.0	6.9
AC006064.6	0.0	0.0	3.4
TAP2	0.0	0.0	3.2
CYP1A1	0.0	0.0	1.7
FOSB	0.0	0.0	1.4
IL1B	0.0	0.0	1.3
CXCL8	0.0	0.0	1.1
CXCL2	0.0	0.0	1.1
CYP1B1	0.0	0.0	1.0

C

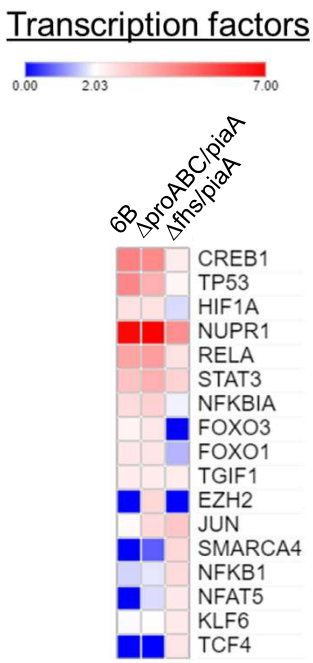

D

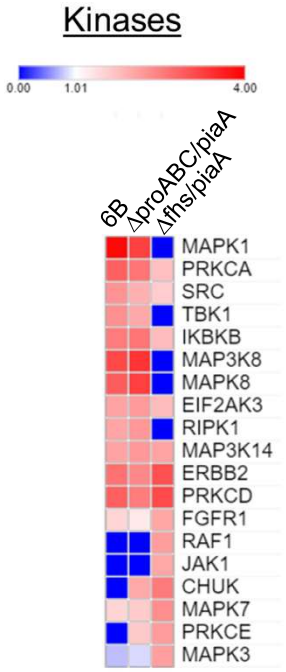

E

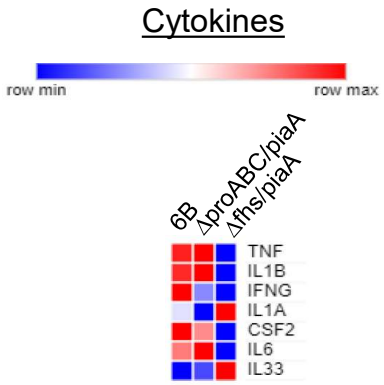

F

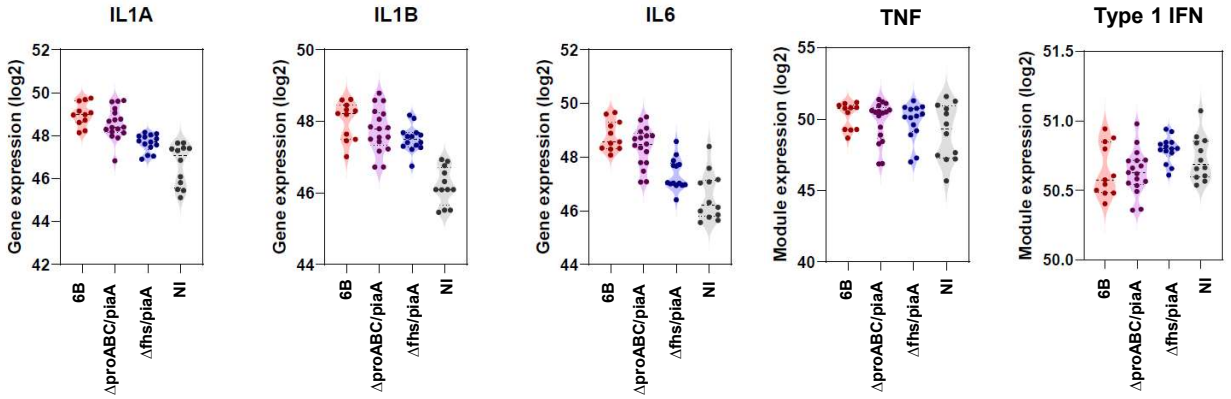

Figure 6

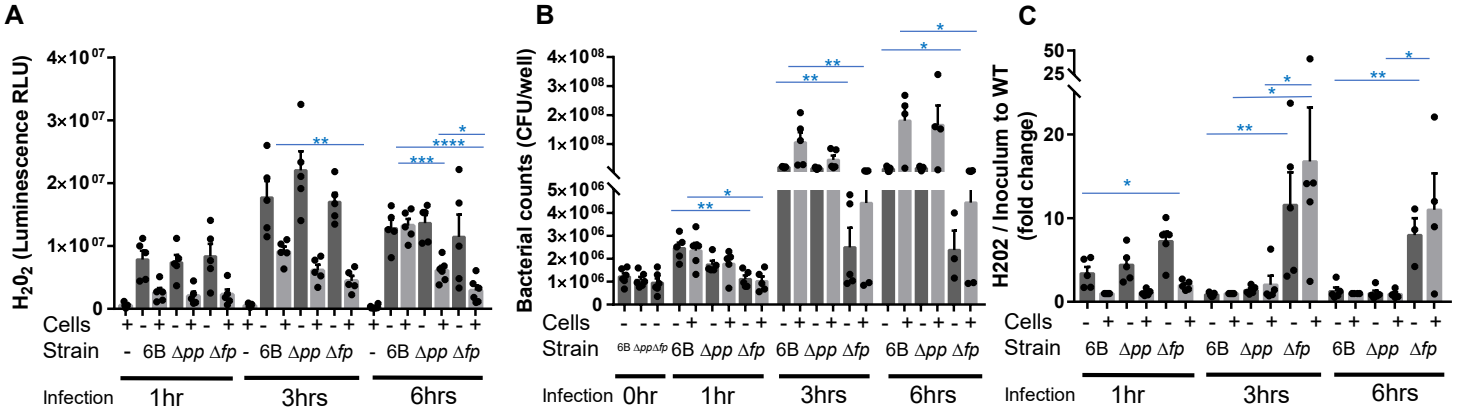
A
H_2O_2 (Luminescence RLU)
4×10^07
3×10^07
2×10^07
1×10^07
0
Cells
Strain
- 6B Δpp Δfp - 6B Δpp Δfp - 6B Δpp Δfp
Infection
1hr
3hrs
6hrs
B
Bacterial counts (CFU/well)
4×10^08
3×10^08
2×10^08
1×10^08
5×10^06
4×10^06
3×10^06
2×10^06
1×10^06
0
Cells
Strain
6B ΔppΔfp 6B Δpp Δfp 6B Δpp Δfp 6B Δpp Δfp
Infection
0hr
1hr
3hrs
6hrs
C
H202 / Inoculum to WT (fold change)
50
25
20
10
0
Cells
Strain
6B Δpp Δfp 6B Δpp Δfp 6B Δpp Δfp
Infection
1hr
3hrs
6hrs

Figure 7

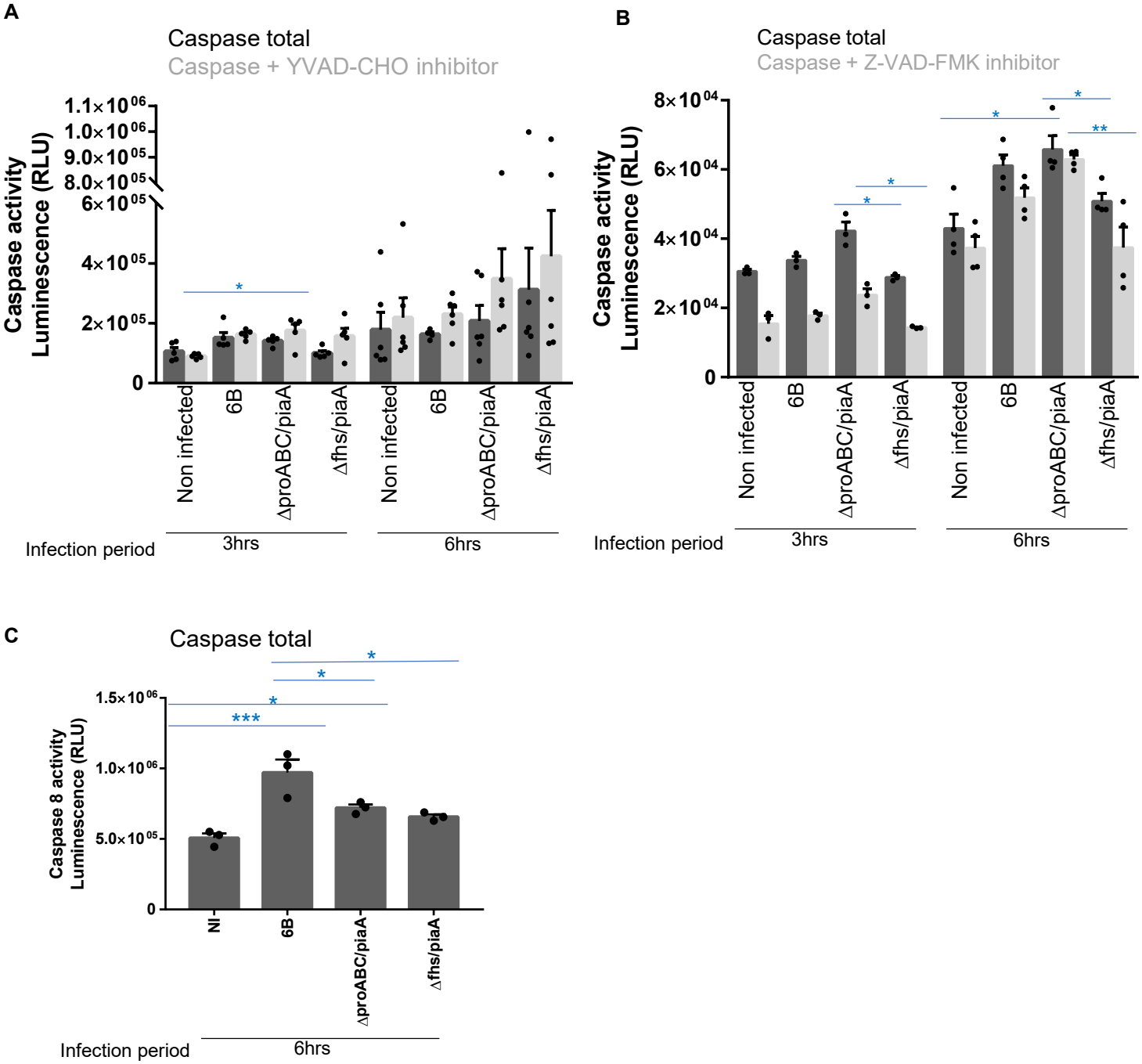
A
Caspase total
Caspase + YVAD-CHO inhibitor
Caspase activity
Luminescence (RLU)
1.1×10^06
1.0×10^06
9.0×10^05
8.0×10^05
6×10^05
4×10^05
2×10^05
0
*
Non infected
6B
ΔproABC/piaA
Δfhs/piaA
Non infected
6B
ΔproABC/piaA
Δfhs/piaA
Infection period
3hrs
6hrs
B
Caspase total
Caspase + Z-VAD-FMK inhibitor
Caspase activity
Luminescence (RLU)
8×10^04
6×10^04
4×10^04
2×10^04
0
*
**
Non infected
6B
ΔproABC/piaA
Δfhs/piaA
Non infected
6B
ΔproABC/piaA
Δfhs/piaA
Infection period
3hrs
6hrs
C
Caspase total
Caspase 8 activity
Luminescence (RLU)
1.5×10^06
1.0×10^06
5.0×10^05
0
***
*
NI
6B
ΔproABC/piaA
Δfhs/piaA
Infection period
6hrs
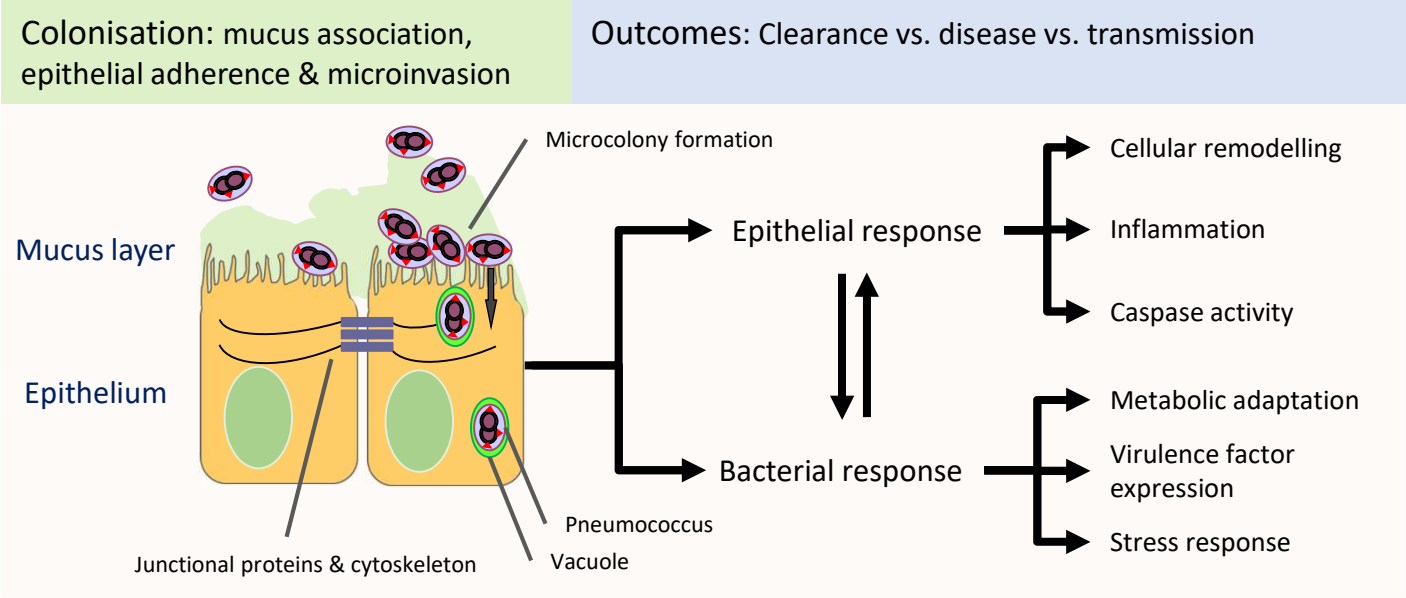
Graphical abstract